Petroleum Science 23 (2026) 2527–2544

Contents lists available at ScienceDirect

Petroleum Science

journal homepage: www.keaipublishing.com/en/journals/petroleum-science

Original Paper

An anisotropy-dynamic ant colony optimization with probabilistic fracture uncertainty quantification for sub-seismic fault detection

Shi-Chang Li [a], Yang Zhao [a,*], Cheng-Gang Xian [a], Qi-Ya Qiao [b], Fu-Yu Zhu [a], Xing Liang [c], Jie-Hui Zhang [c], Lan-Lan Yan [d]

[a] State Key Laboratory of Petroleum Resources and Engineering, China University of Petroleum (Beijing), Beijing, 102249, China
[b] Beijing Geological Environment Monitoring Institute, Beijing, 100195, China
[c] PetroChina Zhejiang Oilfield Company, Hangzhou, 311100, Zhejiang, China
[d] Geophysical Research Institute, SINOPEC, Nanjing, 211103, Jiangsu, China

ARTICLE INFO

Article history:
Received 29 June 2025
Received in revised form
1 November 2025
Accepted 11 February 2026
Available online 17 February 2026

Edited by Meng-Jiao Zhou

Keywords:
Ant colony optimization
Fracture detection
Azimuthal anisotropy
Hidden Markov Model (HMM)
Uncertainty quantification

ABSTRACT

The precise characterization of subsurface fracture systems, especially sub-seismic fractures below seismic resolution, is critical for developing complex hydrocarbon reservoirs. While ant colony optimization (ACO) introduced "ant tracking" for seismic fracture detection, traditional methods rely on isotropic post-stack attributes, ignoring azimuthal anisotropy—a key indicator of fracture orientation and density. The azimuth-aware anisotropic bayes ACO (Ani-Bayes ACO) integrated pre-stack anisotropy via Bayesian priors but suffered from deterministic constraints and static heuristics, limiting its ability to model conjugate fracture systems or parameter uncertainty. To resolve these limitations, we propose the anisotropy-dynamic ACO (ADACO) algorithm. ADACO replaces deterministic constraints with probabilistic, dynamically evolving fracture parameter distributions: von Mises for orientation and log-normal for density, both parameterized by elliptical fitting credibility. During optimization, a Hidden Markov Model (HMM) globally evaluates path consistency, while elite-path feedback iteratively focuses the distributions. This enables uncertainty-quantified fracture prediction, multi-set tracking, and autonomous adaptation to fracture clustering. Validation in a complex shale gas reservoir showed 85% consistency with drilling data—a significant improvement over Ani-Bayes ACO (46%). ADACO thus provides a robust tool for sub-seismic fracture characterization.

1. Introduction

The precise characterization of subsurface fracture systems, particularly the fine-scale delineation of sub-seismic fractures that extend from meters to tens of meters and lie far below the vertical seismic resolution (typically $< \lambda/4$), represents a core challenge in the efficient development of structurally complex hydrocarbon reservoirs (Zhang et al., 2024c). Although individually undetectable on seismic profiles, the interconnected networks formed by these fractures collectively govern reservoir permeability, fluid migration pathways, and ultimately, the efficacy of hydraulic fracturing operations (Liu et al., 2025; Zhang, 2023). The spatial patterns of these fracture networks are governed by a dual control of regional tectonic stress history and lithological heterogeneity (Asrillah et al., 2024). Therefore, constructing accurate, cross-scale, 3D models of these features is the critical bridge connecting macroscopic seismic structural interpretation with microscopic rock physics properties (Liu et al., 2024; Zhang et al., 2024b).

To address this challenge, a diverse suite of algorithms has been developed. Classical image processing techniques, such as Hough transforms and edge-detection filters, are computationally efficient but often suffer from high sensitivity to seismic noise, tending to produce fragmented results (Chen et al., 2025). More recently, deep learning methods, particularly Convolutional Neural Networks (CNNs), have shown power in pattern recognition but are critically dependent on vast, high-quality, manually labeled

* Corresponding author.
E-mail address: zhaoyang@cup.edu.cn (Y. Zhao).
Peer review under the responsibility of China University of Petroleum (Beijing).

http://dx.doi.org/10.1016/j.petsci.2026.02.016

training datasets—a significant bottleneck for the subtle, sub-seismic features targeted in this study (An et al., 2021; Ashtari, 2025).

In this context, the classic "ant tracking" technique, based on ant colony optimization (ACO), offers a compelling alternative. This swarm intelligence method simulates the path-finding behavior of artificial agents ("ants") that navigate the seismic volume, depositing digital "pheromones" to reinforce paths along high-discontinuity features identified by post-stack geometric attributes like curvature (Choi et al., 2024; Prakash et al., 2023). This agent-based, self-organizing mechanism provides inherent robustness to incoherent noise and is designed to identify continuous pathways (Acuña-Uribe et al., 2021; Ashraf et al., 2020; Cheng et al., 2022). However, the traditional ACO framework is fundamentally constrained by key limitations, with one of the most critical being an intrinsic "isotropic" assumption. Specifically, the requisite stacking process discards crucial azimuthal seismic information, rendering the data insensitive to azimuthal anisotropy—a key physical indicator of fracture orientation and density (Dong et al., 2022; Guo et al., 2022; Li et al., 2021).

To address the isotropy issue, the Ani-Bayes ACO (ABACO) method integrated pre-stack azimuthal anisotropy as prior knowledge within a Bayesian decision framework (Li et al., 2023; Tsvankin et al., 2010; Zhang and Li, 2024). While this marked a significant milestone by introducing directional intelligence, ABACO's architecture is built upon two critical theoretical flaws. First, it treats the results of elliptical fitting as a single, deterministic mean value, an oversimplification that fails to represent inherent parameter uncertainty, especially in geologically complex areas with conjugate fracture systems. Second, its use of a static heuristic and a fixed Bayesian prior lack the adaptability to handle spatially variant data quality, compromising the reliability of the tracking results and motivating the need for a fully dynamic approach.

Building upon this foundation and to resolve these theoretical dilemmas, we propose a novel anisotropy-dynamic ACO (ADACO) algorithm. The core idea of ADACO is a paradigm shift: replacing the deterministic, static constraints of previous methods with a probabilistic, dynamically evolving model of fracture parameters (Mavrovouniotis et al., 2020; Skackauskas et al., 2022; Zhou et al., 2022). Specifically, ADACO encodes elliptical fitting results into probability distributions that represent uncertainty—using the von Mises distribution for orientation and the log-normal for density, both parameterized by data credibility. During optimization, a Hidden Markov Model (HMM) globally evaluates path consistency, while feedback from elite paths continuously refines the prior distributions, guiding the algorithm's convergence. This hierarchical framework endows ADACO with three transformative capabilities: (1) uncertainty-quantified prediction of fracture intensity, (2) simultaneous tracking of competing fracture sets, and (3) autonomous adaptation to multi-scale fracture clustering. Field data validation in a tectonically complex shale gas reservoir demonstrates ADACO's superior ability to resolve sub-seismic fracture corridors, achieving a consistency of 85% with drilling data—a significant improvement over the 46% achieved by Ani-Bayes ACO. This work thus provides a more powerful and reliable tool for the characterization of sub-seismic subsurface fracture systems.

This evolutionary perspective provides the necessary context for the detailed technical exposition that follows. The upcoming Methods section will first briefly revisit the foundational principles of Classic ACO, then detail the Ani-Bayes ACO framework upon which our work builds, and finally, present a comprehensive exposition of the anisotropy-dynamic ACO algorithm. This tripartite approach will systematically demonstrate how ADACO's architecture overcomes the limitations of its predecessors. Subsequently, the Results section will leverage field data to empirically demonstrate the performance enhancements of ADACO in fracture tracking, solidifying its practical value.

2. Methodology

The fracture detection framework proposed in this study, anisotropic dynamic ant colony optimization (ADACO), represents a systematic evolution of ant-tracking algorithms. To elucidate the theoretical contributions and novel mechanisms of ADACO, this section delineates the methodology following a progressive narrative. We begin by detailing the foundational geophysical attributes and the formulation of traditional ant colony optimization (ACO). We then introduce the concept of integrating pre-stack anisotropy through an intermediate Bayesian framework (Ani-Bayes ACO), highlighting its advancements and inherent limitations. Finally, we present the full ADACO methodology, detailing how it overcomes these limitations through a dynamic, probabilistic approach.

2.1. The traditional isotropic framework: curvature and classic ACO

2.1.1. Curvature attribute as a geometric heuristic

The primary input for traditional ant-tracking algorithms is a seismic attribute that accentuates structural discontinuities. Volumetric curvature, a second-order derivative of the seismic reflection surface, is particularly effective at amplifying localized strata deformation induced by faulting or fracturing (Cao et al., 2025; Zhang et al., 2025). The maximum curvature, $K_{\max}$, is therefore used as a foundational geometric heuristic to guide artificial ants toward zones of high structural complexity (Al-Dossary and Marfurt, 2006).

2.1.2. Traditional ant colony optimization (ACO)

The classic ACO algorithm applies swarm intelligence to navigate the seismic volume (e.g., ant tracking technology). Artificial agents deposit pheromones (τ) along their paths, with routes corresponding to high-discontinuity features—as indicated by the curvature attribute ($\eta_{\text{curvature}}$)—receiving greater reinforcement. The probability (P_{ij}) for an ant to transition from its current node i to a neighboring node j is governed by the standard rule:

$$P_{ij} = \frac{\left[\tau_{\text{ij}}\right]^{\alpha} \cdot [\eta_{\text{curvature}}(j)]^{\beta}}{\sum_{k \in \Omega_i} [\tau_{ik}]^{\alpha} \cdot [\eta_{\text{curvature}}(k)]^{\beta}} \tag{1}$$

where Ω_i is the set of neighboring nodes to i, α and β are parameters controlling the influence of the pheromone and heuristic, respectively.

This traditional approach, however, is fundamentally limited. By relying solely on post-stack geometric attributes, the search process is inherently isotropic and blind to the crucial directional

information encoded in fracture-induced azimuthal anisotropy. Furthermore, its use of static heuristics often leads to an over-emphasis on strong geometric anomalies, thus failing to detect sub-seismic fractures with weaker signatures.

2.2. The anisotropic advancement: azimuthal data and Ani-Bayes ACO

To address the isotropic limitation, an intermediate advancement involves integrating pre-stack seismic information. This approach is necessary because curvature and azimuthal anisotropy measure fundamentally different aspects of rock deformation. Curvature captures the macroscopic geometric expression of deformation—the bending and breaking of rock layers. In contrast, azimuthal anisotropy reveals the intrinsic rock fabric modified by stress and fracturing; it is a direct physical measurement of how seismic waves travel differently in different directions due to aligned cracks. Therefore, while curvature highlights where deformation has occurred, anisotropy indicates the orientation and intensity of the resulting fracture network, providing critical information that is absent in post-stack data. This makes the integration of azimuthal anisotropy not just an improvement, but a necessity for moving towards a more physically realistic fracture characterization.

2.2.1. Fracture-induced azimuthal anisotropy

In horizontally transverse isotropic (HTI) media, P-wave velocity varies with azimuth. This phenomenon is quantified by fitting an ellipse to velocity data from azimuthally sectored gathers (Durrani et al., 2023; Xie et al., 2020):

$$V_{\mathrm{p}}(\phi_i) = A + B\cos[2(\phi_i - \phi_0)] \tag{2}$$

where $V_{\mathrm{P}}(\phi_i)$ is the P-wave velocity observed at a specific azimuth, ϕ_i is the observation azimuth for the ith sector, A represents the average P-wave velocity over all azimuths, B quantifies the magnitude of the velocity variation (the anisotropy strength), and ϕ_0 is the fast-velocity azimuth. This analysis yields three key parameters:

- Fracture orientation (ϕ_0): The azimuth of the ellipse's major axis, interpreted as the dominant fracture strike.
- Fracture density (e): A measure of the anisotropy magnitude. Geologically, a higher fracture density value (e) suggests a greater concentration of aligned fractures within a given rock volume. Following P-wave anisotropy theory (Bakulin et al., 2000; Cao et al., 2024), it can be defined as the relative difference between the fast ($V_{\mathrm{Pfast}} = A + B$) and slow ($V_{\mathrm{Pslow}} = A - B$) velocities:

$$e = \frac{V_{\mathrm{Pfast}} - V_{\mathrm{Pslow}}}{V_{\mathrm{Pfast}}} = \frac{2B}{A+B} \tag{3}$$

- Credibility (c): A metric evaluating the goodness-of-fit. It is calculated from the ratio of the elliptical fitting residual to the total data variation, providing a quantitative measure of the reliability of the HTI assumption and the derived parameters:

$$c = 1 - \frac{\sum_{i=1}^{N}\left[V_{\mathrm{p}}(\phi_i)^{\mathrm{obs}} - V_{\mathrm{p}}(\phi_i)^{\mathrm{fit}}\right]^2}{\sum_{i=1}^{N}\left[V_{\mathrm{p}}(\phi_i)^{\mathrm{obs}} - \overline{V}_{\mathrm{p}}^{\mathrm{obs}}\right]^2} \tag{4}$$

where $V_{\mathrm{p}}^{\mathrm{obs}}$ is the observed velocity, V_{p}^{fit} is the fitted value, and $\overline{V}_{\mathrm{p}}^{\mathrm{obs}}$ is the mean of the observed velocities.

2.2.2. Bayesian heuristic design and the Ani-Bayes ACO

The Ani-Bayes ACO (ABACO) framework incorporates this anisotropy information by using the deterministic, point-estimate values of ϕ_0 and e as prior knowledge. The final decision is based on the posterior probability according to Bayes' theorem:

$$P\left(\mathrm{path}_j \middle| \mathrm{strike}\right) \propto P\left(\mathrm{strike} \middle| \mathrm{path}_j\right) \cdot P\left(\mathrm{path}_j\right) \tag{5}$$

where $P\left(\mathrm{path}_j\right)$ is the prior probability (akin to the traditional ACO probability) and $P\left(\mathrm{strike} \middle| \mathrm{path}_j\right)$ is the likelihood, which quantifies how well the path aligns with the fracture strike φ_0. This makes the algorithm directionally intelligent.

While a significant improvement, ABACO's methodology has critical flaws that motivate the present work. Its reliance on a single, deterministic elliptical fit constitutes an oversimplified anisotropy model. Moreover, by using only the mean values, it completely discards vital information about the uncertainty and spatial variability of these parameters, making it susceptible to converging on local anisotropy "highs".

2.3. The proposed method: Ani-Dynamic ACO (ADACO)

To overcome predecessors' limitations, the Ani-Dynamic ACO (ADACO) framework adopts a probabilistic, dynamic, and globally optimized process. Its comprehensive workflow (Fig. 1) starts with "Foundational components for fracture tracking"—extracting post-stack curvature and pre-stack anisotropy attributes (detailed in Sections 2.1 and 2.2). These attributes serve as the crucial initial inputs that are transformed and utilized within the algorithm's core: an iterative optimization loop composed of four key modules: (1) probabilistic anisotropy encoding, (2) dynamic heuristic sampling, (3) HMM-based path evaluation, and (4) iterative distribution focusing. To provide a clear, step-by-step computational procedure that complements the conceptual flowchart in Fig. 1, the complete ADACO process is formally outlined in Algorithm 1. This pseudocode details the implementation of each module, highlighting the novel contributions within the full iterative loop.

The workflow begins with the extraction of post-stack (e.g., curvature) and pre-stack (anisotropy) attributes. The core of the algorithm is an iterative process composed of four key modules: (1) encoding the anisotropy information into probability distributions, (2) dynamically sampling these distributions to form a stochastic heuristic, (3) evaluating candidate paths globally using a Hidden Markov Model (HMM), and (4) focusing the initial distributions based on feedback from elite paths. This loop continues until convergence, yielding a robust and detailed sub-seismic fracture network.

Algorithm 1: The anisotropy-dynamic ant colony optimization (ADACO) framework

Input: Post-stack seismic cube (for curvature), pre-stack azimuthal data, ACO parameters (α, β_1, β_2), HMM parameters (γ), Iteration limit (k_{max})

Output: Optimized 3D fracture network

// Initialization phase

Calculate curvature attribute from post-stack data.

Perform elliptical fitting on pre-stack data to obtain fracture orientation (ϕ_0), density (e), and credibility (c).

FOR each node in the seismic volume:

// [Novelty 1: Probabilistic anisotropy encoding]

Initialize von Mises distribution $P(\theta|\mu,\kappa)$ for orientation using φ_0 and c.

Initialize log-normal distribution $P(x|\mu_{ln},\sigma_{ln})$ for density using e and c.

Initialize pheromone trail τ uniformly.

END FOR

// Iterative optimization phase

FOR $k = 1$ to k_{max}:

  FOR each ant $m = 1$ to M:

    // Path construction

    Select a starting node.

    WHILE path is not complete:

      // [Novelty 2: Dynamic heuristic sampling]

      At current node i, for each neighbor j:

        Sample a density value x_j.

        Compute anisotropic heuristic.

        Calculate transition probability.

      Move ant to the next node based on P_{ij}.

    END WHILE

  END FOR

  // Path evaluation and update phase

  // [Novelty 3: HMM-based global path evaluation]

  FOR each completed path:

    Calculate global path fitness score using the HMM forward algorithm.

  END FOR

  Identify the elite path (path with the highest HMM fitness).

  // [Novelty 4: Iterative distribution focusing]

  FOR each node i on the elite path:

    Update parameters (μ, κ) of the von Mises distribution.

    Update parameters (μ_{ln}, σ_{ln}) of the log-normal distribution.

  END FOR

  Update pheromone trails based on HMM fitness scores.

END FOR

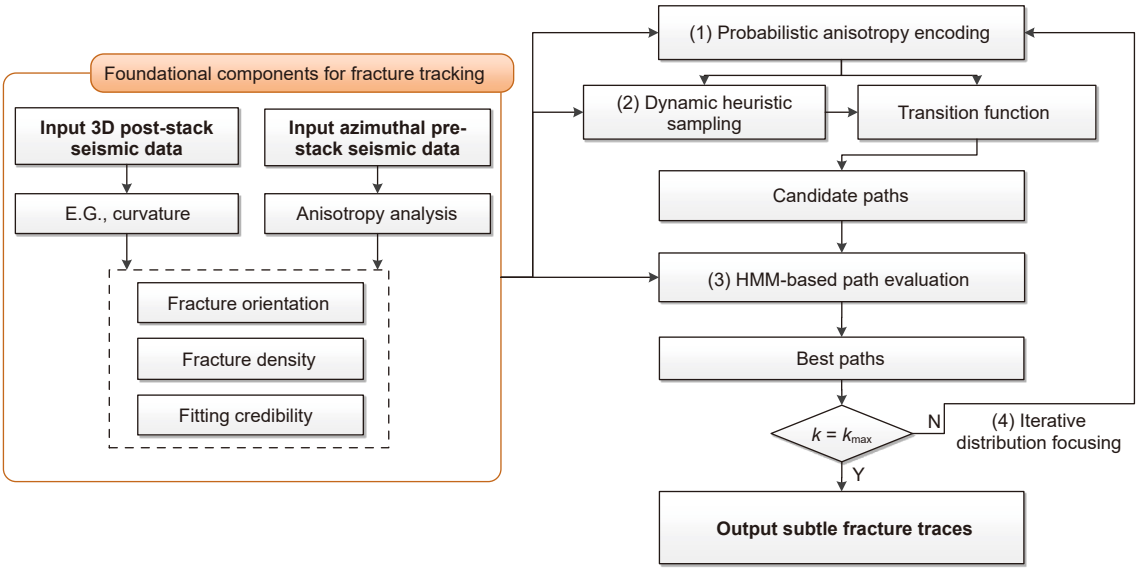

Fig. 1. Flowchart for the Ani-Dynamic ACO (ADACO).

2.3.1. Probabilistic anisotropy encoding: from determinism to uncertainty

A pivotal flaw in previous anisotropy-guided methods is the deterministic treatment of elliptical fitting results. The derived fracture orientation (ϕ_0) and density (e) are used as absolute values, ignoring the fact that their reliability, quantified by the fitting credibility (c), varies significantly across the seismic volume. A high credibility ($c \to 1$) indicates that the observed azimuthal data conforms well to the simple HTI model, lending credibility to the extracted parameters. However, a low credibility value ($c \to 0$) is not merely an indicator of poor data quality; it is a critical piece of diagnostic information. It can signify geologically complex scenarios where the single-HTI assumption is violated, such as the presence of multiple, non-orthogonal fracture sets, or regions with high levels of incoherent noise. Treating a low-credibility parameter estimate with the same certainty as a high-credibility one introduces significant bias and can lead to erroneous fracture interpretations.

This inherent, spatially-variant uncertainty necessitates a paradigm shift away from deterministic point estimates. ADACO addresses this by pioneering a probabilistic encoding scheme. Instead of using the raw parameter values, we use them—along with their associated credibility—to parameterize probability distributions. This approach does not discard low-credibility information but rather uses it to correctly represent a higher degree of uncertainty. This probabilistic foundation is the cornerstone of ADACO's robustness and adaptability.

- Fracture orientation is modeled using the von Mises distribution:

$$P(\theta|\mu,\kappa) = \frac{e^{\kappa \cos(\theta-\mu)}}{2\pi I_0(\kappa)} \tag{6}$$

The choice of the von Mises distribution is physically motivated; as fracture orientation is circular data (where 0° and 360° are identical), this distribution, often called the "Circular Normal", is the natural choice over linear distributions like the Gaussian. Its mean parameter (μ) directly represents the dominant fracture strike (ϕ_0), while the concentration (κ) quantifies the certainty of this orientation (scaled by the credibility c). High credibility yields a large κ and a sharply peaked distribution, while low credibility leads to a small κ and a wider distribution, acknowledging higher uncertainty. $I_0(\kappa)$ denotes the modified Bessel function of order 0.

Fig. 2 illustrates how the shape of the von Mises distribution, parameterized by the ellipse-fitted fracture direction and its corresponding credibility, represents fracture orientation characteristics. The distribution's peak position is controlled by μ. For example, a distribution with $\mu = 0°$ peaks at 0° (blue line), while one with $\mu = 45°$ peaks at 45° (orange line). This peak position directly reflects the dominant fracture orientation identified by ellipse fitting. The concentration parameter (κ), derived from credibility (e.g., $\kappa = k_0 \cdot c$, where k_0 is a scaling factor), governs the distribution's spread. When credibility is high (as $c \to 1$), κ is large, resulting in a sharp, unimodal peak (green line, $\kappa = 10$). This high concentration of fracture directions typically indicates a dominant fracture set, often associated with a single tectonic phase. Conversely, low credibility (as $c \to 0$) leads to κ approaching 0 and a nearly uniform distribution (blue line, $\kappa = 1$), signifying high uncertainty in the fitted direction. A low κ value can reflect either the

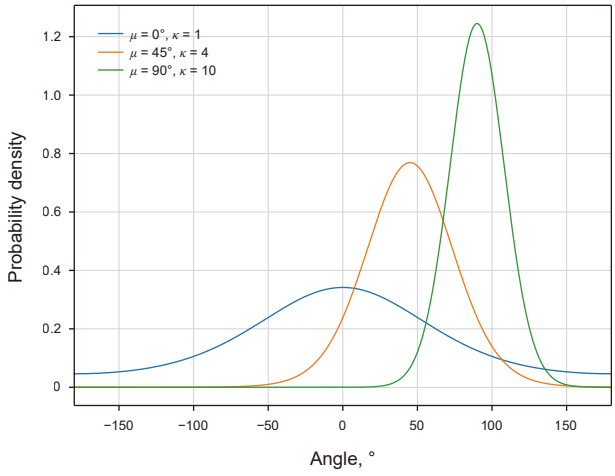

Fig. 2. Von Mises distributions with varying parameters.

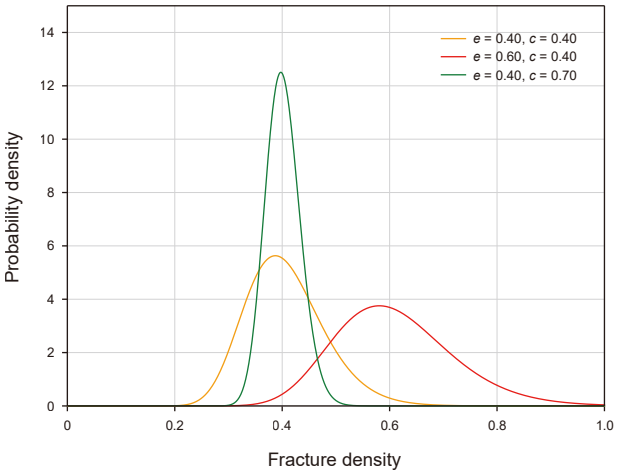

Fig. 3. Log-normal distributions with varying parameters.

presence of multiple intersecting fracture sets (potentially from polyphase tectonic activity) or be indicative of high data noise.

- Fracture density is modeled using the log-normal distribution:

$$P(x|\mu_{\ln},\sigma_{\ln}) = \frac{1}{x\sigma_{\ln}\sqrt{2\pi}} e^{-\frac{(\ln x-\mu_{\ln})^2}{2\sigma_{\ln}^2}} \quad (7)$$

Fracture density is a non-negative quantity that often exhibits a right-skewed statistical distribution in geological settings (i.e., many low-to-moderate values with a tail of high values). The log-normal distribution accurately captures both of these physical and statistical properties. The log-mean $\mu_{\ln}$ is related to the density value e, and the log-standard deviation $\sigma_{\ln}$ is inversely proportional to the credibility c.

Fig. 3 illustrates how variations in the Log-Normal distribution parameters—the log-mean ($\mu_{\ln}$) and log-standard deviation ($\sigma_{\ln}$)—influence fracture density characteristics. The log-mean governs the distribution's central tendency and overall position, directly related to the ellipse-fitted fracture density (e). Higher fitted density values correspond to a larger $\mu_{\ln}$, shifting the distribution towards higher densities (red line) and indicating an increased probability of high fracture density. This may suggest brittle lithologies (e.g., sandstone) or proximity to structurally active zones (e.g., faults). Conversely, lower fitted density results in a smaller $\mu_{\ln}$, shifting the distribution towards lower densities (yellow line) and potentially indicating plastic rock layers (e.g., mudstone) or tectonically stable areas. The log-standard deviation controls the distribution's spread and the uncertainty in the density estimate; it is inversely related to the ellipse fitting credibility. High credibility ($c\to1$) corresponds to a small $\sigma_{\ln}$ (approaching 0), resulting in a narrow distribution (green line) and high credibility in the estimated density. This narrowness may suggest relatively uniform fracture development. Conversely, low credibility ($c\to0$) leads to a large $\sigma_{\ln}$ (approaching σ_0), yielding a wide, right-skewed distribution (yellow line). This indicates significant uncertainty in the ellipse fitting results and may reflect heterogeneity in fracture density, potentially due to alternating fracture clusters and matrices.

This probabilistic representation provides a much richer and more geologically realistic set of prior information, as summarized in Tables 1 and 2.

Table 1 matches the mathematical features of these log-normal (for fracture density) and von Mises (for fracture orientation) distributions to their geophysical meanings. Table 2 illustrates resulting fracture scenarios under various parameter combinations. Crucially, mapping fitting credibility to distribution parameters quantifies the uncertainty in direction and density estimates. This probabilistic representation significantly benefits the ACO heuristic: the initial azimuthal anisotropy distributions guide the search towards high-probability zones, reducing computational waste, while wider distributions for low-credibility data buffer against noise. This approach provides a more robust framework for fracture tracing, aligning with geophysical data statistics and offering richer prior information for path generation by dynamically adjusting distribution shapes based on data reliability.

2.3.2. Dynamic heuristic sampling

A cornerstone of any ACO algorithm is the heuristic information (η) that guides an ant's decision at each step. In traditional methods, this heuristic is static, typically assigning η_{ij} to a pre-computed attribute value (e.g., curvature or mean fracture density) at the target node j. This static approach is fundamentally flawed as it treats these attributes as infallible ground truth, ignoring the uncertainty inherent in their calculation and their failure to capture the geological context of path continuity.

ADACO rectifies this by introducing a dynamic heuristic sampling model. Instead of using a fixed heuristic value, the guidance for a transition from a current node i to a candidate node j is stochastically generated *in-situ* for each ant. This is achieved by sampling from the local, confidence-aware probability distributions established in Section 2.3.1. This process ensures that each decision is informed not only by the most likely fracture properties but also by their associated uncertainty and the geological principle of directional consistency.

The anisotropic heuristic, $\eta_{\text{aniso}}(i,j)$, is formulated as a composite of two probabilistically evaluated factors:

Table 1
The geophysical meaning of key distribution parameters.

Distribution parameter	Mathematical characteristic	Geophysical meaning
Von Mises μ	Distribution peak azimuth	Main fracture strike
Von Mises κ	Concentration (distribution width)	Consistency of fracture direction: High value – single stress field; Low value – multiple tectonic periods or noise
Lognormal $\mu_{\ln}$	Lognormal mean (density mean)	Degree of fracture development: High value – brittle rock layer or tectonic active zone; Low value – ductile rock layer or stable area
Lognormal $\sigma_{\ln}$	Lognormal standard deviation (dispersion)	Density heterogeneity: High value – fractured basement and bedrock interface; Low value – homogeneous mudstone layer

Table 2
Tectonic scenarios for different parameter combinations.

Scenario	Von Mises distribution	Log-normal distribution	Geological interpretation
High confidence, single fracture set	$\mu = 45°$, $\kappa = 8$	$\mu_{\ln} = 1.5$, $\sigma_{\ln} = 0.2$	Clear main fracture strike, high and uniform density, indicating a fracture system formed by a single tectonic event.
Low confidence, multiple fracture sets	$\mu = 90°$, $\kappa = 0.5$	$\mu_{\ln} = 0.8$, $\sigma_{\ln} = 1.0$	Dispersed direction (multiple sets of conjugate fractures), large variation in density, possibly due to multiple tectonic events or complex stress fields.
Medium confidence, fracture development zone	$\mu = 120°$, $\kappa = 3$	$\mu_{\ln} = 2.2$, $\sigma_{\ln} = 0.5$	Relatively consistent fracture direction, high density but with local fluctuations, corresponding to fault-associated fracture zones.

1. Stochastic fracture density: A fracture density value, x_j, is randomly drawn from the log-normal distribution $P\left(x \mid \mu_{\ln,j}, \sigma_{\ln,j}\right)$ at the destination node j. This sampling internalizes uncertainty: in low-credibility regions (large $\sigma_{\ln,j}$), the broader distribution permits a wider range of explored values, preventing the algorithm from being misguided by an unreliable point estimate.
2. Directional coherence: The geological plausibility of the path segment from i to j is assessed. The azimuth of this segment, θ_{ij}, is evaluated against the von Mises distribution $P(\theta \mid \mu_i, \kappa_i)$ centered at the current node i. This term, $P\left(\theta_{ij} \mid \mu_i, \kappa_i\right)$, quantifies how well the proposed step aligns with the locally dominant fracture strike, promoting the formation of continuous, geologically realistic paths.

The anisotropic heuristic is then defined as the product of the sampled density and its directional likelihood:

$$\eta_{\text{aniso}}(i,j) = x_j \cdot P\left(\theta_{ij} \mid \mu_i, \kappa_i\right), \tag{8}$$

where x_j

$$\sim \text{Log} - \text{normal}\left(\mu_{\ln,j}, \sigma_{\ln,j}\right)$$

This dynamic heuristic is then integrated with the conventional geometric heuristic (curvature) and pheromone level to form the final transition probability rule, providing a multi-faceted guidance mechanism:

$$P_{ij} = \frac{\left[\tau_{ij}\right]^{\alpha} \cdot [\eta_{\text{aniso}}(i,j)]^{\beta_1} \cdot [\eta_{\text{curvature}}(j)]^{\beta_2}}{\sum_{k \in \Omega_i} [\tau_{ik}]^{\alpha} \cdot [\eta_{\text{aniso}}(i,k)]^{\beta_1} \cdot [\eta_{\text{curvature}}(k)]^{\beta_2}} \tag{9}$$

Here, β_1 and β_2 are weighting parameters. This dynamic sampling transforms the heuristic from a static, deterministic input into an intelligent, adaptive process. It intrinsically balances exploration (by sampling from wider distributions in uncertain areas) with exploitation (by favoring high-probability directions and densities), guiding ants toward robust and geologically sound fracture networks.

2.3.3. HMM-based global path evaluation

In classic ACO frameworks, the fitness of a completed path is typically assessed using a simple cumulative metric, such as the sum of heuristic values along its nodes. This local, additive approach is fundamentally myopic. It is incapable of evaluating the path as a coherent geological object, often rewarding paths that are locally attractive but globally discontinuous or implausible.

To overcome this critical deficiency, ADACO introduces a superior path evaluation mechanism based on a Hidden Markov Model (HMM). The HMM provides a probabilistic framework for analyzing sequences, making it exceptionally well-suited to assess the geological integrity of an entire ant path from a global perspective. Instead of summing local attributes, the HMM calculates the total likelihood of the observed sequence of fracture attributes along the path, given the underlying sequence of state transitions (i.e., directional choices). This yields a holistic fitness score that quantifies the global coherence of the entire fracture trace.

The HMM is defined by its core components, adapted for fracture tracking:

- Hidden states (S): The hidden states correspond to the directional choices available to an ant. At each node i along a path, the state s_{ik} represents the decision to move in a specific direction θ_{ik}.
- Observations (O): For each ant, the observation sequence is the series of stochastically sampled fracture density values, $x_1, x_2, \ldots, x_T$, that were generated during the path construction phase (Section 2.3.2). The observation at node i along a specific ant's path is therefore its unique sampled value, x_i.
- Transition probability (A): The transition probability between an adjacent node i and node j must holistically evaluate the continuity of the geological system. A more robust metric than evaluating a single path direction is to measure the similarity between the entire fracture orientation distributions at the two nodes. To this end, we employ the Kullback-Leibler (KL) divergence, a fundamental measure from information theory that quantifies the difference between two probability distributions. A lower divergence signifies higher similarity in the fracture systems. The transition probability $A_{i,j}$ is therefore defined using an exponential kernel, which transforms the dissimilarity (divergence) into a similarity score. This probability is independent of the specific start and end states and depends only on the node properties, reflecting the continuity of the underlying geological environment:

$$A_{i,j} = \exp\left(-\gamma \cdot D_{\text{KL}}\left(\text{VM}_i \parallel \text{VM}_j\right)\right) \tag{10}$$

where VM_i and VM_j are the von Mises distributions at nodes i and j respectively, and γ is a positive scaling parameter. For two von Mises distributions, $\text{VM}(\theta|\mu, \kappa)$, the KL divergence has a closed-form solution:

$$D_{\text{KL}}\left(\text{VM}_i \parallel \text{VM}_j\right) = \ln\left(\frac{\text{I}_0\left(\kappa_j\right)}{\text{I}_0(\kappa_i)}\right) + \kappa_i\left(\frac{\text{I}_1(\kappa_i)}{\text{I}_0(\kappa_i)}\right)\cos\left(\mu_i - \mu_j\right) - \kappa_j \cos\left(\mu_i - \mu_j\right) \tag{11}$$

Here, I_0 and I_1 are modified Bessel functions of the first kind. This formulation ensures that the HMM rewards paths that traverse regions of consistent fracture orientation systems.

- Emission probability (B): The emission probability links the hidden state (the chosen direction) to the observed sampled

density. For a given ant's path, the probability of having observed the sampled value x_i at node i is calculated using the log-normal probability density function at that node:

$$B_i(k) = P\left(x = x_i \middle| \mu_{\ln,i}, \sigma_{\ln,i}\right) = \frac{1}{x_i\ \sigma_{\ln,i}\ \sqrt{2\pi}}\ \mathrm{e}^{-\frac{\left(\ln x_i - \mu_{\ln,i}\right)^2}{2\sigma_{\ln,i}^2}} \tag{12}$$

- Initial state probability (π): The probability of starting in a given state s_{1k} is proportional to the emission probability at the first node.

For any given path (an observation sequence O and state sequence S), the overall joint likelihood, $P(O,S|\lambda)$, where $\lambda = (A, B, \pi)$, can be calculated efficiently using the forward algorithm. This likelihood serves as a robust, globally-aware fitness score. Paths that exhibit both high directional consistency (high transition probabilities) and alignment with high-density zones (high emission probabilities) will naturally receive a higher fitness score. This score is subsequently used to modulate the pheromone update, ensuring that only globally coherent and geologically plausible fracture networks are reinforced over successive iterations.

2.3.4. Iterative distribution focusing

The probabilistic encoding and dynamic sampling mechanisms provide ADACO with powerful exploratory capabilities, crucial for avoiding premature convergence to local optima. However, unconstrained exploration can be computationally inefficient. To create a virtuous feedback loop that balances exploration with exploitation, ADACO incorporates a final, adaptive mechanism: Iterative distribution focusing. This process uses the knowledge gained from the best-performing paths in one iteration to refine the guiding probability distributions for the next, effectively focusing the search on increasingly promising regions of the solution space.

After each iteration, the parameters of the von Mises and log-normal distributions are updated for all nodes belonging to the "elite" path (the path with the highest HMM-derived fitness). This mechanism mimics a learning process, where the algorithm gains "confidence" in specific fracture characteristics as it discovers globally coherent structures.

1. Fracture density distribution update: The log-normal distribution parameters are updated to favor the density characteristics of the elite path. The log-mean $\mu_{\ln}$ is nudged towards the sampled density on the path, and the log-standard deviation $\sigma_{\ln}$ is reduced to decrease uncertainty, thereby focusing the search.

$$\mu_{\ln,\mathrm{j}}^{(t+1)} = (1-\eta_\rho)\mu_{\ln,\mathrm{j}}^{(t)} + \eta_\rho \ln\left(x_j^{(t)}\right)$$

$$\sigma_{\ln,\mathrm{j}}^{(t+1)} = \max\left(\sigma_{\ln,\mathrm{j}}^{(t)} \cdot \delta, \sigma_{\min}\right) \tag{13}$$

where t is the iteration number, $x_j(t)$ is the density sampled at node j on the elite path, η_ρ is a learning rate, δ is an exponential decay factor ($0 < \delta < 1$), and $\sigma_{\min}$ is a floor value to prevent over-focusing and maintain minimal exploration.

2. Fracture orientation distribution update: The von Mises parameters are updated to reinforce directions that form globally coherent paths. The mean direction μ is steered towards the direction of the elite path segment, and the concentration κ is increased to sharpen the directional preference.

$$\mu_i^{(t+1)} = \mathrm{angle}\left((1-w)\cdot\ \mathrm{e}^{i\mu_i^{(t)}} + w\cdot\ \mathrm{e}^{i\theta_{ij}^{(t)}}\right)$$

$$\kappa_i^{(t+1)} = \kappa_i^{(t)} + \zeta\cdot\ \mathrm{fitness(path)} \tag{14}$$

where $\theta_{ij}(t)$ is the direction of the elite path segment leaving node i, w is a weight factor controlling the update speed of the mean direction, and ζ is a scaling factor that links the update strength to the path's fitness (fitness(path), the HMM-computed global likelihood, as detailed in Section 2.3.3).

This iterative focusing mechanism simulates a geological maturation process, enabling a progressively more accurate utilization of fracture azimuthal anisotropy. The algorithm initiates with broad distributions representing high initial uncertainty. Subsequently, a feedback loop, gated by the HMM's global sequence evaluation, ensures that only geologically consistent elite paths are selected to iteratively sharpen these guiding distributions. This mechanism provides a decisive advantage over classic ACO's direct pheromone update. Instead of merely reinforcing a specific path—a process prone to premature convergence (stagnation)—our "property-based" reinforcement learns and sharpens the underlying geological properties (e.g., density and orientation) of the elite path. This dynamic adaptation not only focuses the computational search on validated, high-potential fracture trends but also encourages the exploration of other, parallel, undiscovered paths that share the same successful characteristics. The result is a more robust global search, efficient convergence, and a final network that is a precise and reliable reflection of the underlying anisotropic rock fabric.

2.3.5. Parameter settings

The successful implementation of the ADACO algorithm depends on the careful selection of several key parameters. The parameters governing the iterative distribution focusing mechanism are particularly sensitive, as they control the exploration-exploitation trade-off. To determine their optimal values, we conducted a systematic sensitivity analysis on a representative sub-volume of the data, using the final HMM fitness score as the primary performance metric.

For the fracture density distribution update, the learning rate (η_ρ) and decay factor (δ) were analyzed (Fig. 4). A high learning rate (>0.3) caused premature convergence, while a low rate (<0.05) resulted in inefficient learning; 0.1 provided the optimal balance. Similarly, an aggressive decay factor (<0.95) trapped the algorithm in local optima, whereas 0.98 offered a gradual and robust reduction in uncertainty, maximizing the final fitness score.

A similar analysis was performed for the fracture orientation distribution update parameters (w and ζ), which dictate the adaptation of the directional search. The results (Fig. 5) indicate that a weight (w) of 0.2 prevents both overly aggressive steering and sluggish adaptation. An optimal concentration factor (ζ) of 0.05 was found to allow a steady increase in directional confidence without prematurely eliminating alternative orientations.

The empirically determined optimal values for all key parameters used in this study are explicitly listed in Table 3.

2.4. Methodological evolution summary

To concisely summarize the methodological evolution, Fig. 6 illustrates the conceptual workflows of traditional ACO, Ani-Bayes ACO (ABACO), and the proposed Ani-Dynamic ACO (ADACO) (see Table 4). This comparison illustrates the evolution in data utilization and the progressive refinement of the optimization strategy.

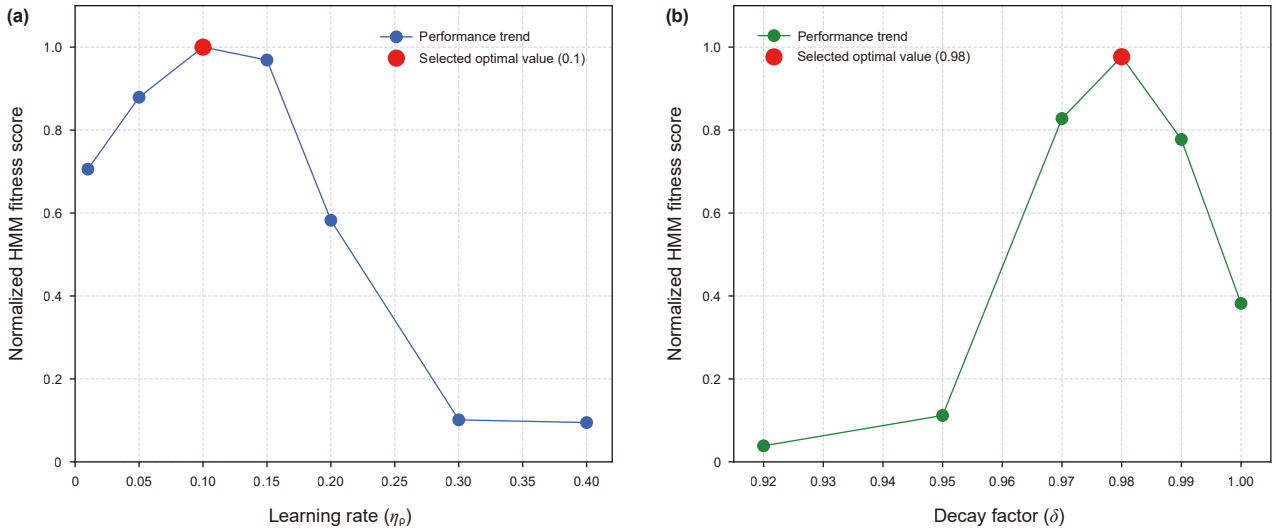

Fig. 4. Sensitivity analysis for fracture density distribution update parameters. **(a)** Learning rate sensitivity, **(b)** decay factor sensitivity.

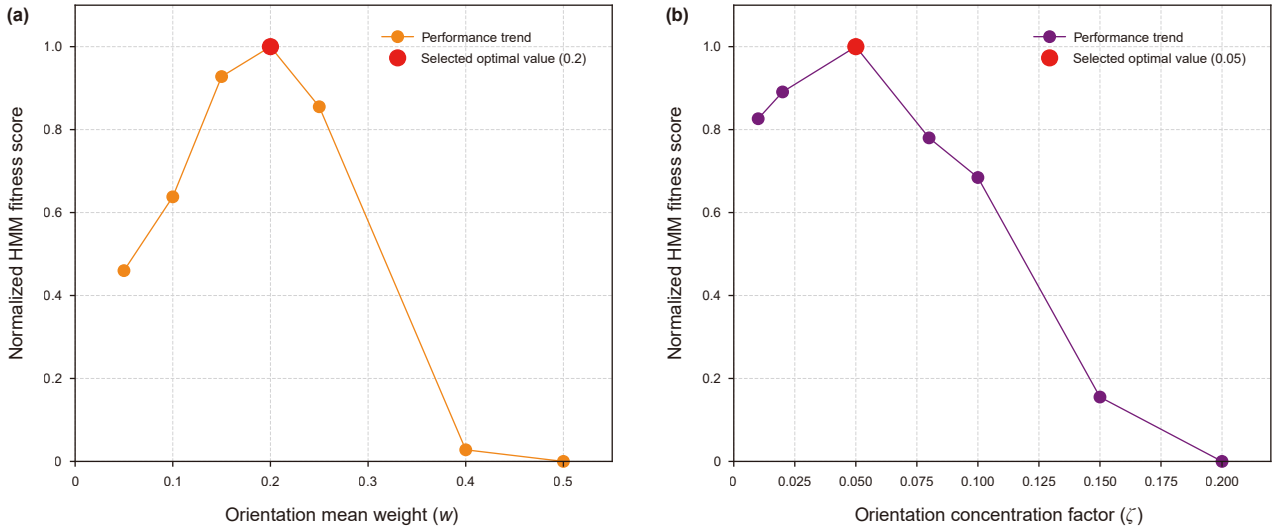

Fig. 5. Sensitivity analysis for fracture orientation distribution update parameters. **(a)** Orientation mean weight sensitivity, **(b)** orientation concentration factor sensitivity.

Table 3
Key parameters and their settings for the ADACO algorithm.

ACO core parameters	Symbol	Value
Pheromone influence factor	α	1
Curvature heuristic factor	β_1	3
Anisotropic heuristic factor	β_2	5
Pheromone evaporation rate	ρ	0.5
Number of ants	M	2000
Maximum iterations	$k_{\max}$	50
HMM parameter		
KL divergence scaling factor	γ	0.8
Focusing parameters		
Density update learning rate	η_ρ	0.1
Density update decay factor	δ	0.98
Min. density std. dev.	$\sigma_{\min}$	0.1
Orientation update weight	w	0.2
Orientation update factor	ζ	0.05

The traditional ACO workflow (Fig. 6(a)) is a process founded entirely on post-stack geometric attributes. Its inherent limitation is an isotropic search mechanism that is oblivious to the directional rock physics information contained in pre-stack data. The ABACO method (Fig. 6(b)) represents a significant advancement by incorporating azimuthal anisotropy. However, it treats the results of elliptical fitting as deterministic inputs for a Bayesian framework with a static heuristic, making it susceptible to local optima and unable to account for parameter uncertainty.

The proposed ADACO workflow (Fig. 6(c)) fundamentally enhances this process by introducing a dynamic optimization loop with direct geological analogues. It overcomes prior limitations through four interconnected innovations. First, probabilistic anisotropy Encoding quantifies parameter uncertainty using confidence-aware distributions. This model then informs dynamic

Table 4
Evolution of ant colony optimization (ACO) algorithms for seismic fracture detection, comparing algorithmic mechanisms and geological applications.

Dimension	Traditional ACO	Ani-Bayes ACO	Ani-Dynamic ACO
Algorithm	Ant colony	Bayesian-constrained path selection	Probabilistic dynamic optimization with multi-attribute fusion
Data	Post-stack attributes	Post-stack attributes + OVT pre-stack azimuths	Post-stack attributes + OVT pre-stack azimuths
Anisotropy modeling		Deterministic ellipse-fitting (fracture intensity/strike)	Probabilistic distributions (log-normal density + von Mises strike) with uncertainty weighting
Fracture density		Intensity-driven search allocation	Probabilistic density mapping with confidence-based prioritization
Heuristic design	Static curvature	Bayesian prior-guided heuristics	Dynamic sampling + non-stationary HMM for global path optimization
Directional constraints	Isotropic search	Fixed-angle constraints from ellipse-fitting	Adaptive directional constraints (iterative consistency refinement)
Path evaluation	Local node attribute accumulation	Posterior probability updates	Full-path geological continuity modeling via non-stationary HMM
Parameter adaptation	Fixed evaporation rate	Global pheromone updates based on fracture intensity	Adaptive distribution refinement ($\mu/\sigma/\kappa$ optimization)
Fracture detection	Macro-scale fault	Meter-scale fractures	Multi-scale fracture networks (noise-resilient, sub-$\lambda/4$ detection)
Ideal application	Simple fracture corridors	Coherent fracture clusters (single dominant orientation)	Multi-phase zones-fracture systems (strike-slip/thrust interactions)

heuristic sampling, which generates an adaptive, path-specific guide for the ant search. Subsequently, HMM-Guided path evaluation enforces geological consistency by assessing entire paths for alignment with tectonic principles. Finally, iterative distribution focusing provides adaptive convergence, mimicking fracture maturation to progressively lock onto dominant structures. This transforms the linear process into an intelligent, adaptive loop that converges on a globally optimized and physically realistic fracture model.

3. Results

To rigorously evaluate the performance of the proposed Ani-Dynamic ant colony optimization (ADACO) algorithm, we applied it to a 3D seismic dataset from the Zhaotong structural zone, Southwest China. The results are presented in a progressive sequence, demonstrating how each algorithmic enhancement, informed by richer geophysical data, leads to a more accurate fracture characterization.

3.1. Geological and structural framework: The challenge of a complex reservoir

The reservoir target is the fractured shallow marine shales of the Ordovician Wufeng to Silurian Longmaxi Formations. This region's tectonic setting is defined by its location on the northern flank of the Haiba anticline, which has undergone multiple, superimposed phases of tectonic activity (Zhang et al., 2024a). The strata have been subjected to repeated episodes of compression, extension, and shear, resulting in an extremely complex and highly

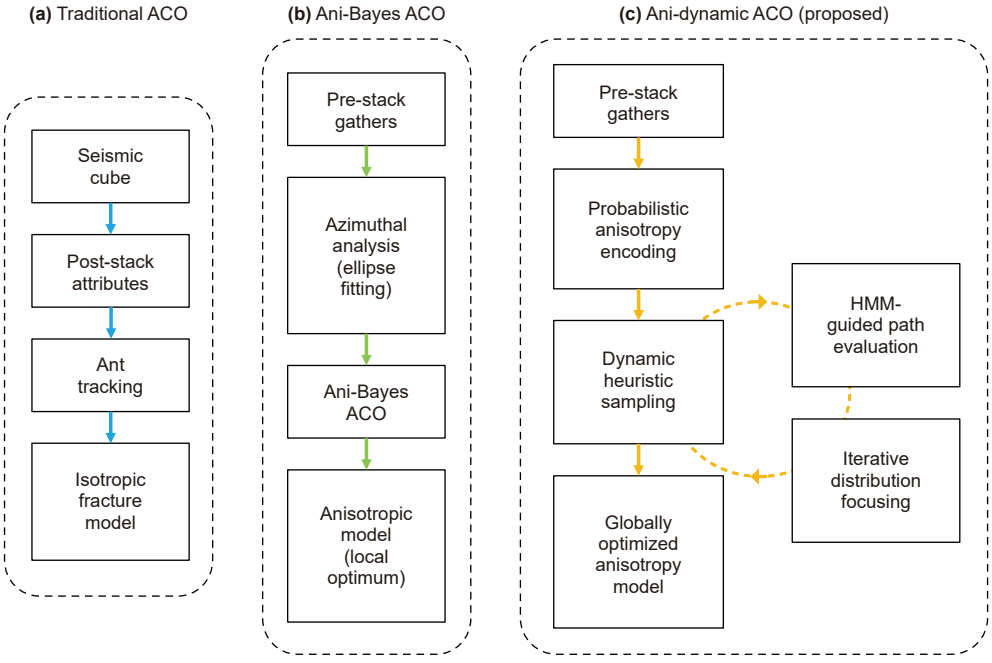

Fig. 6. Conceptual workflows comparing **(a)** traditional ACO, **(b)** Ani-Bayes ACO (ABACO), and **(c)** the proposed Ani-Dynamic ACO (ADACO). The ADACO workflow introduces a dynamic, iterative loop (dashed line) that leverages probabilistic encoding, global HMM evaluation, and adaptive focusing to overcome the limitations of the preceding linear, deterministic approaches.

heterogeneous fracture network (Fig. 7). This intricate structural history is the primary challenge for reservoir characterization. Consequently, an accurate understanding of the orientation, density, and spatial distribution of these fractures is paramount for effective well placement and the optimization of production strategies. This geological complexity necessitates advanced geophysical methods that can look beyond simple structural mapping.

3.2. Post-stack analysis: curvature attribute and the traditional ACO baseline

The initial analysis relied solely on post-stack seismic data, a common industry practice. The maximum curvature attribute was calculated to highlight structural discontinuities. Fig. 8(a) provides a 3D perspective view of the horizon, facilitating the visualization of its structural configuration and relief. The horizon occurs at depths ranging from approximately 400 to 1000 m. Fig. 8(b) presents a plan view of the horizon, displaying major faults and the locations of wells Y9 and Y1. The curvature attribute effectively enhances structural discontinuities by amplifying the second-order derivative information within the post-stack seismic data. As shown in Fig. 8, high curvature anomalies (blue zones) align precisely with the principal fault traces, clearly delineating zones of intense structural deformation. Therefore, this attribute serves as a valuable tool for initial fracture assessment and provides the foundational structural context for the subsequent tracking algorithms.

A traditional ant colony optimization (ACO) algorithm, using only curvature as a heuristic, was initially applied (Fig. 13(a)). While this approach highlighted the large-scale structural framework, its geological utility is severely limited. The resulting effective resolution is coarse, delineating only major faults (>500 m) while missing finer-scale secondary systems. Critically, the method cannot identify geologically vital damage zones between major faults, misinterpreting these complex fracture patterns as noise. This failure to capture sub-seismic detail prevents establishing a clear genetic or spatial link between the fracture network and principal faults. Thus, this result serves as a baseline, demonstrating the inadequacy of this approach for detailed fracture characterization.

3.3. Anisotropy-guided tracking: introducing pre-stack attributes with ABACO

To overcome the limitations of the post-stack approach, we introduced pre-stack azimuthal anisotropy information. This process begins with the direct observation of velocity variations with azimuth.

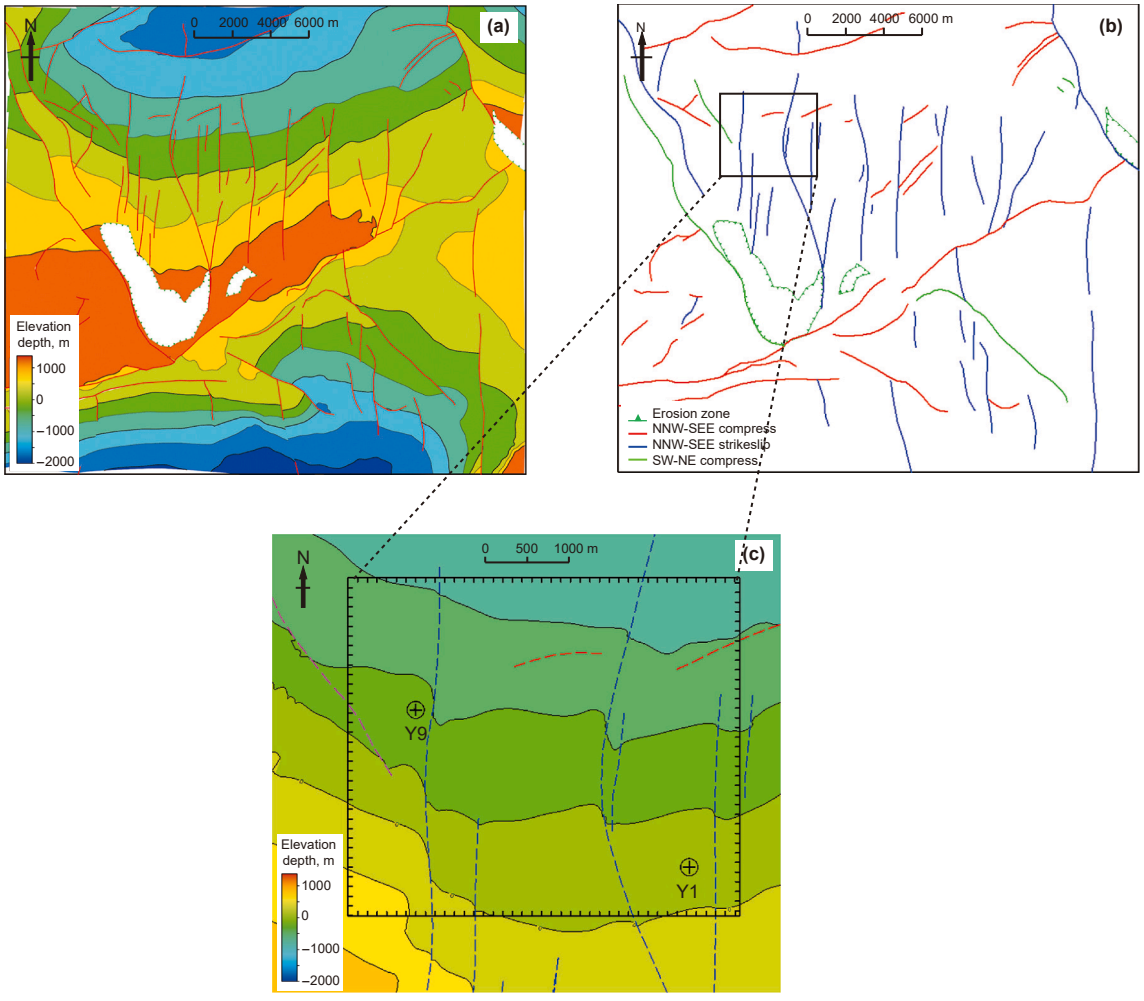

Fig. 7. Structural framework of the study area. **(a)** Structural map of the top Wufeng Formation. **(b)** Interpreted fault systems from different tectonic phases, illustrating the complexity. **(c)** A focused view of the study area with two wells.

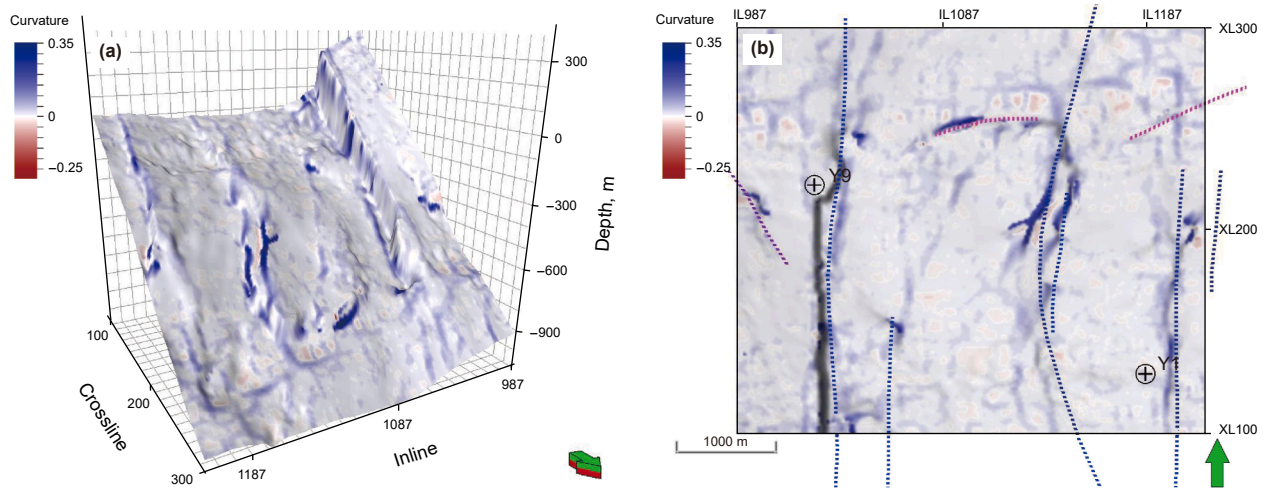

Fig. 8. Maximum curvature attribute of the target horizon. **(a)** A 3D perspective view illustrating the structural relief of the target layer. **(b)** A 2D planar view where high-curvature anomalies (blue zones) correlate strongly with major fault traces (dashed lines), indicating zones of intense deformation and providing a foundational map for fracture tracking. For consistency, this display format, with **(a)** showing a 3D view and **(b)** a 2D view with major faults marked by dashed lines, is maintained for all subsequent attribute figures (Figs. 10–12).

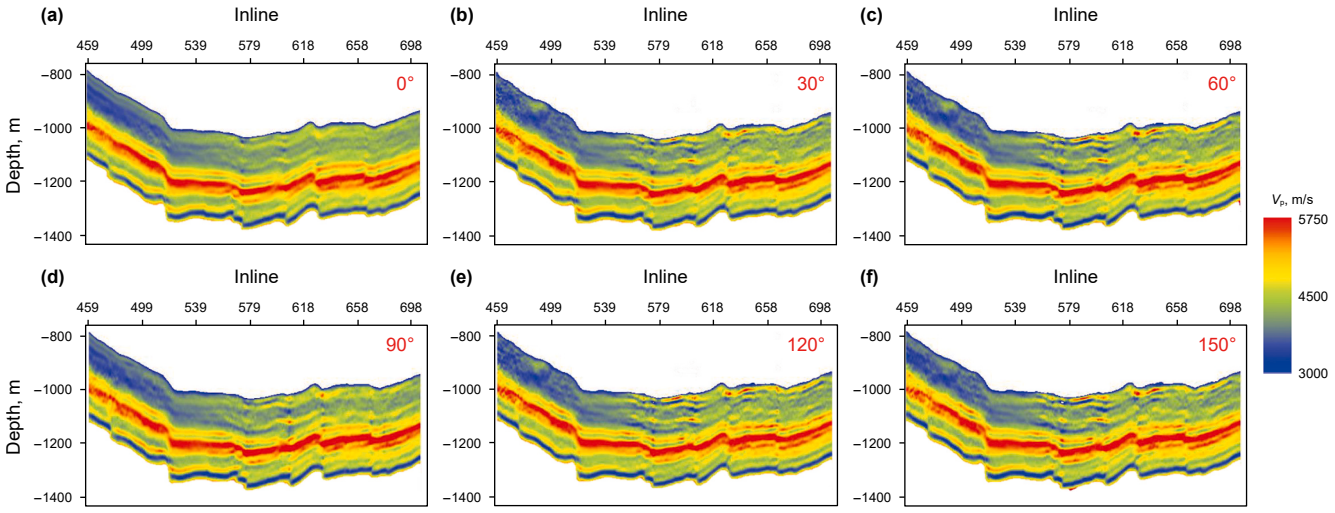

Fig. 9. P-wave velocity inversion profiles at various azimuths. The profiles show clear, systematic variations in velocity at the same depth for different propagation azimuths, providing direct evidence of fracture-induced azimuthal anisotropy.

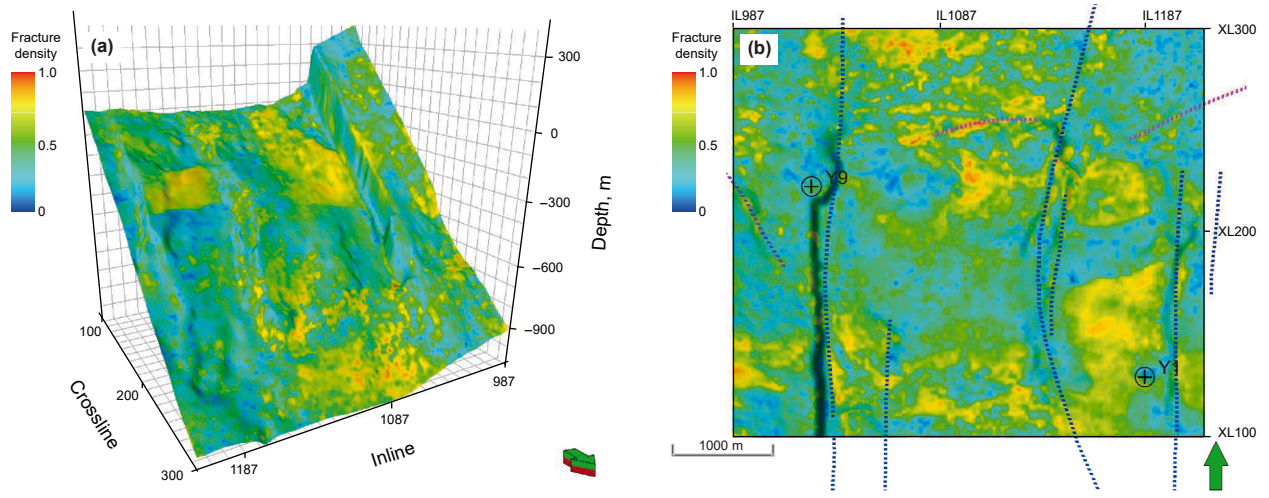

Fig. 10. Fracture density attribute. High-density values (red/yellow) are concentrated near fault zones.

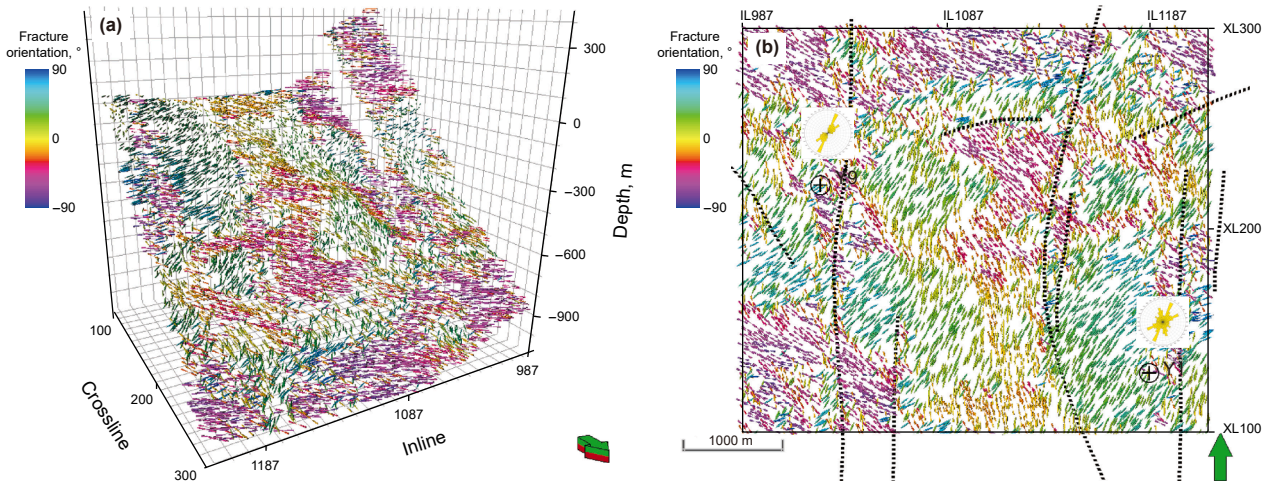

Fig. 11. Fracture orientation attribute. Arrows indicate the dominant fracture strike. Inset rose diagrams show consistency with FMI data.

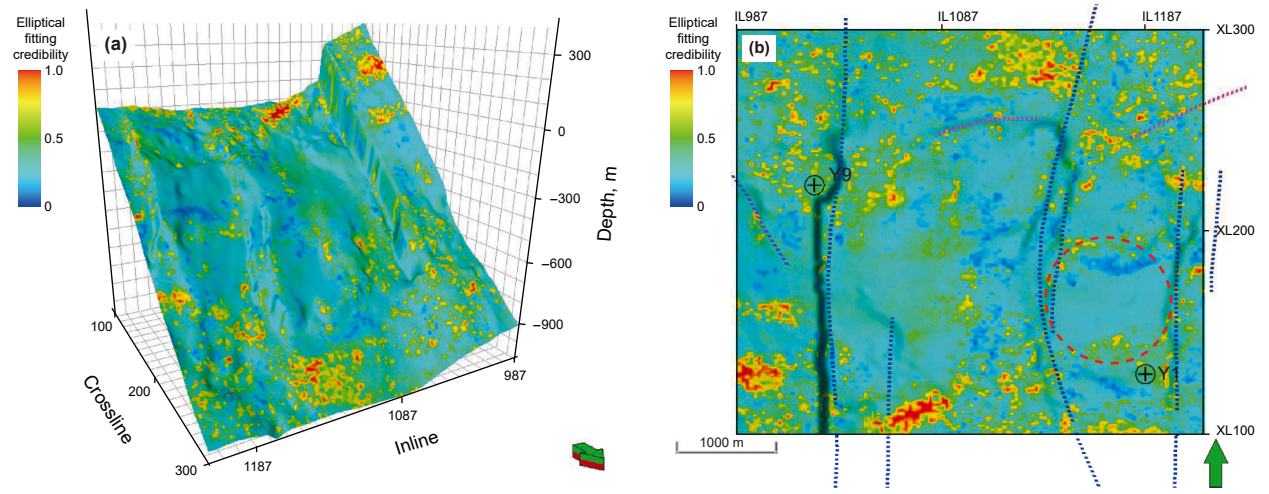

Fig. 12. Elliptical fitting credibility. High credibility (warm colors) indicates a good fit to a single fracture set model, while low credibility (cool colors) suggests complex, multi-directional fracturing.

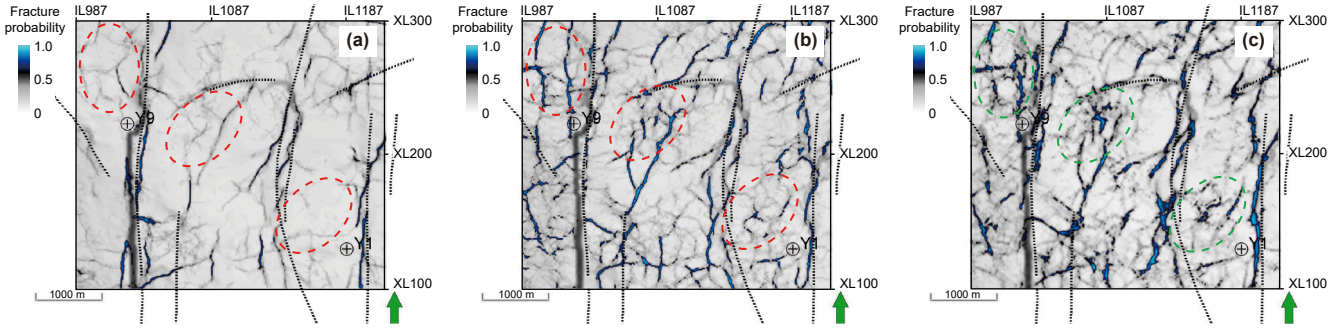

Fig. 13. Comparison of fracture tracking results on the target layer. Planar views of the identified fracture network using **(a)** traditional ACO, **(b)** Ani-Bayes ACO (ABACO), and **(c)** the proposed Ani-Dynamic ACO (ADACO). The progression demonstrates how successively incorporating richer data leads to enhanced resolution and accuracy. Key differences are highlighted for direct comparison: red dashed circles indicate areas where previous methods exhibit limitations, such as fragmented traces, while green solid circles showcase the superior performance of ADACO in resolving these same areas with enhanced connectivity and finer detail.

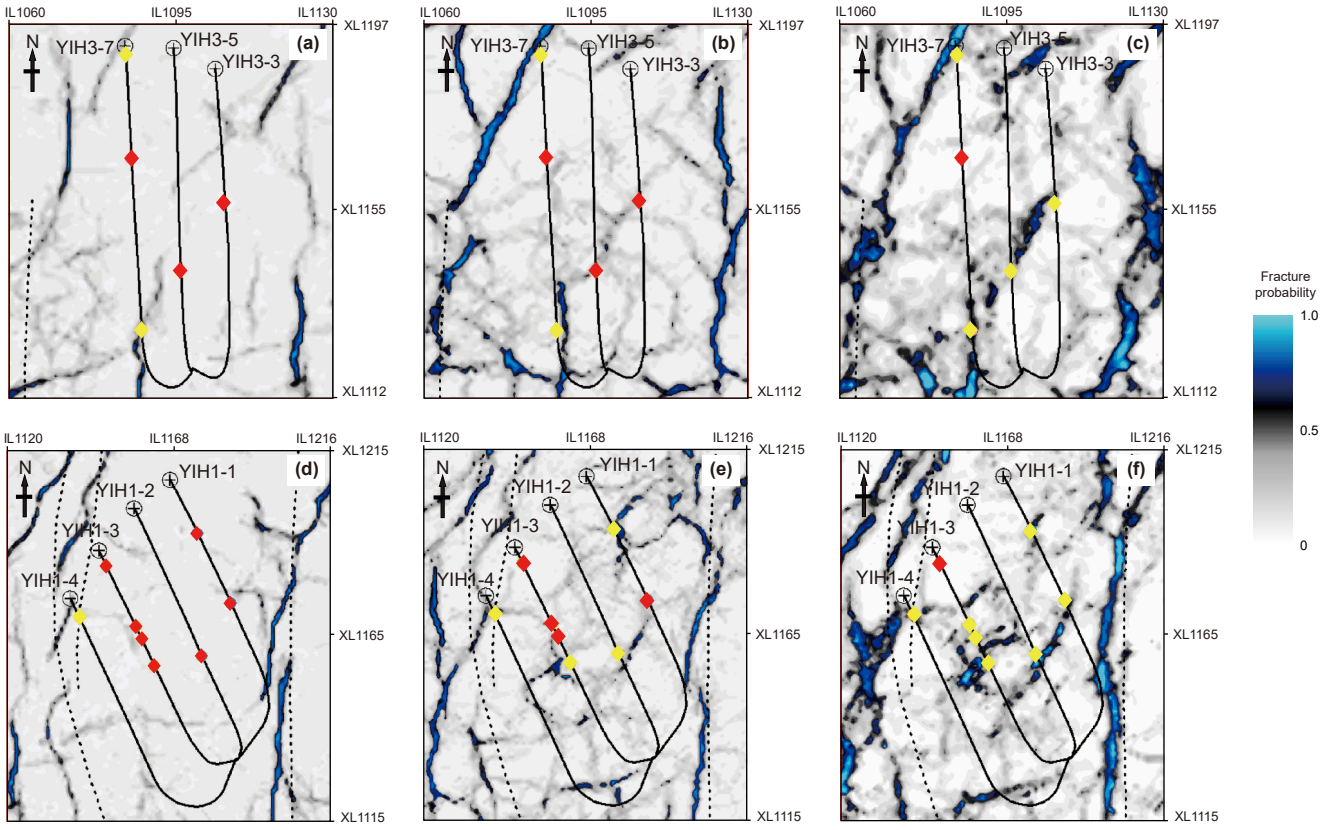

Fig. 14. Comparative validation against drilling data across platforms Y1H1 and Y1H3. The top row **(a)**–**(c)** displays results for Y1H1, while the bottom row **(d)**–**(f)** displays results for Y1H3. Each column represents a different algorithm: traditional ACO ((**a**), (**d**)), ABACO ((**b**), (**e**)), and ADACO ((**c**), (**f**)). Successfully predicted drilled faults are marked with yellow diamonds, while missed faults are marked with red diamonds. The progressive improvement in predictive accuracy and the consistent high performance of ADACO across different areas are clearly demonstrated.

3.3.1. Azimuthal velocity variation: the direct evidence of anisotropy

The raw pre-stack seismic gathers were first partitioned into six azimuthal sectors (0°, 30°, 60°, 90°, 120°, and 150°). AVO inversion was then performed on each sector to yield P-wave velocity profiles. A comparison of these six azimuthal inversion sections (Fig. 9) reveals systematic variations in phase velocity at the same stratigraphic location across different azimuths. For instance, velocity values from the 0° azimuth section exhibit significant differences compared to those from the 90° section. Assuming an HTI medium, these azimuthal velocity variations directly reflect the presence and geometry of fractures. This anisotropic signature is the foundational physical evidence that motivates the use of pre-stack data for improved fracture characterization.

3.3.2. Quantifying anisotropy: Fracture density and orientation

To quantify the observed anisotropy, elliptical fitting was applied to the six azimuthal velocity datasets. Two key parameters were derived: fracture density and fracture orientation. Fig. 10 illustrates the spatial distribution of fracture density, where warm color tones represent higher density. Elevated fracture density is notably observed proximal to faults, particularly at their intersections and terminations, with high-density trends generally aligning with the fault strikes. This strongly indicates that fault activity significantly impacts the fracturing of the surrounding rock mass. Fig. 11 displays the dominant fracture orientations as small, color-coded arrows. The overall pattern reveals that fracture orientations are strongly influenced by the local fault systems. The study area features a co-genetic fracture system dominated by NW-SE and NNE-SSW orientations. At the Y1 and Y9 well locations, these orientations align closely with trends from image log rose diagrams, which confirms the reliability of the fracture analysis. This system originated from a regional N-S dextral strike-slip regime and was amplified by a northern compressive structure. Within the fault damage zones, intense fracturing resulted in a complex, multi-directional mesh of intersecting sets. Conversely, in areas distal to the main faults, the regional stress field produced highly organized fractures, typically arranged in sub-parallel, en echelon, or ladder-like patterns. Together, these two attributes provide direct, physically meaningful information about the fracture system that is absent in isotropic post-stack data.

3.3.3. Ani-Bayes ACO (ABACO) results

We then implemented the Ani-Bayes ACO (ABACO) method, which incorporates fracture density and orientation as a directional constraint (Fig. 13(b)). This yielded a marked improvement over the traditional isotropic approach, enhancing the fracture identification scale to the 200–500 m range and strengthening the algorithm's response within the damage zones adjacent to major faults.

However, the continuity of the tracked fractures remains suboptimal, particularly in areas of complex stress. This limitation is particularly evident near the intersections of major faults where the low fitting credibility (Fig. 12, red-circled aera) suggests the presence of conjugate or multi-directional fracture systems. ABACO's reliance on a single, deterministic mean orientation prevents it from resolving this complexity, resulting in the fragmented and discontinuous paths observed in Fig. 13(b). By failing to account for the parameter uncertainty indicated by low credibility, the algorithm is easily misguided, demonstrating the exact theoretical weaknesses highlighted in the abstract. This reveals a new challenge: how to dynamically account for the inherent uncertainty and heterogeneity within the anisotropy data itself.

3.4. Dynamic, uncertainty-aware tracking: the ADACO breakthrough

The final step addresses the limitations of ABACO by not only incorporating anisotropy but also its associated uncertainty.

3.4.1. Introducing fitting credibility and synthesizing key insights

The credibility of the elliptical fit (Fig. 12) provides a crucial measure of the uncertainty associated with the simplified HTI model. High credibility zones generally coincide with areas of high fracture density, with both attributes decreasing gradually with distance from major faults. However, a critical observation is that in some areas proximal to major faults, high fracture density is accompanied by low fitting credibility. This discrepancy powerfully suggests the presence of complex, multi-directional fracture networks within the fault damage zones, where the assumption of a single dominant fracture set fails. Therefore, fitting credibility is a key indicator of geological complexity, highlighting the need for a more advanced algorithm that can properly weigh this information.

Integrating the insights from curvature and the suite of anisotropy attributes (Figs. 10–12) provides a comprehensive understanding. Major faults act as the primary loci for deformation, promoting associated fracture systems. Curvature helps identify these deformation zones, while azimuthal anisotropy provides a more direct measure of fracture density and orientation. In zones of high curvature, fracture orientations may appear scattered, and fitting credibility may be low, which collectively points to formations subjected to multi-directional deformation that develop interconnected fracture networks of varying scales and orientations. This observed heterogeneity confirms that a simple one-to-one relationship between elliptical fitting and fracture geometry cannot be assumed. In summary, while curvature indicates potential fracture zones, the full suite of azimuthal anisotropy attributes, including credibility, reveals the collective effect and complexity of these sub-seismic scale fractures. This integrated understanding makes a compelling case for a dynamic algorithm like ADACO, which is designed to probabilistically incorporate this uncertainty.

3.4.2. Ani-Dynamic ACO (ADACO) results

The proposed ADACO framework was then applied, demonstrating optimal performance in terms of detail, continuity, and

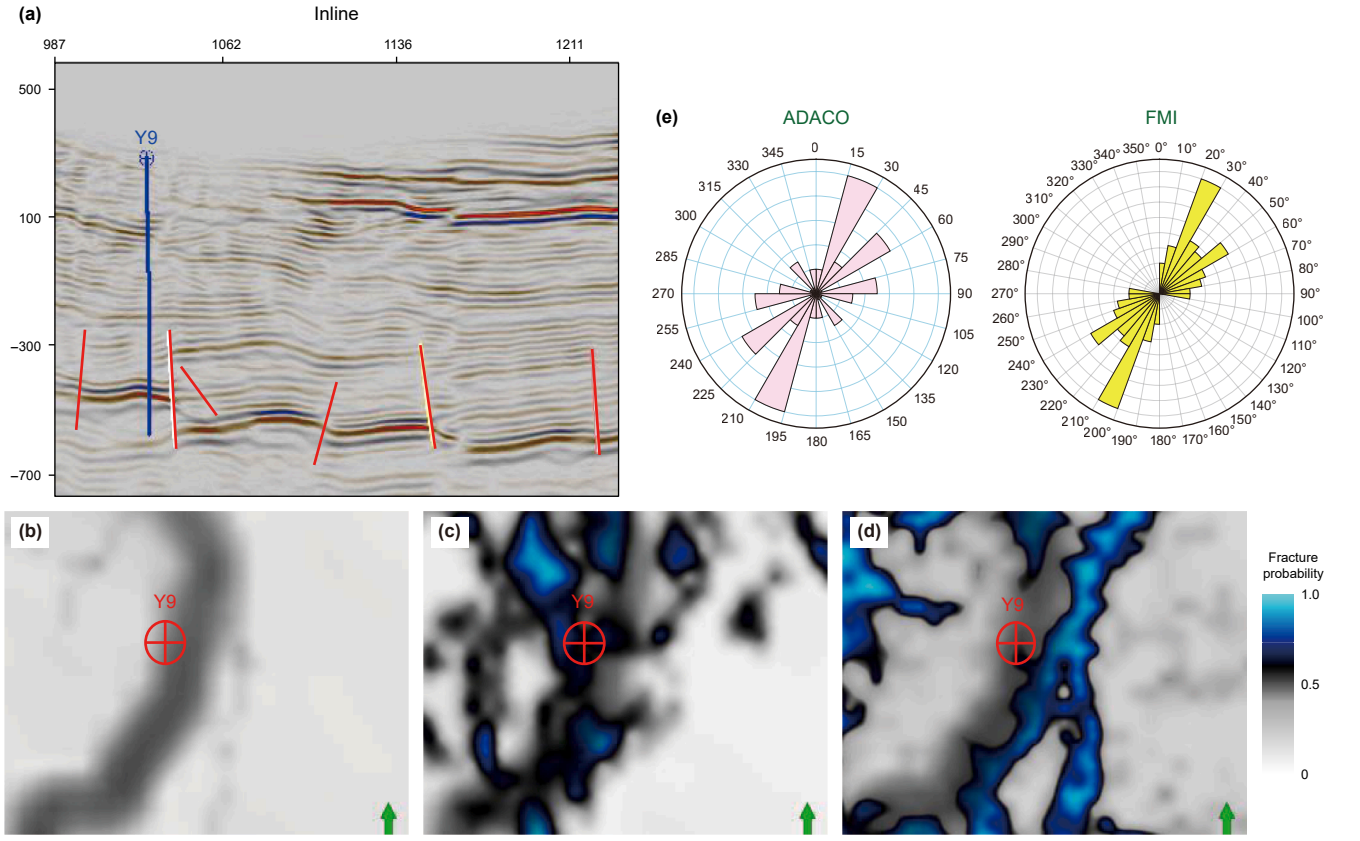

Fig. 15. Integrated validation panel at well Y9, located in a structurally complex setting. **(a)** Seismic profile showing the well trajectory intersecting a syncline with multiple nearby thrust faults. **(b)**–**(d)** Side-by-side comparison of the fracture networks predicted by **(b)** traditional ACO, **(c)** Ani-Bayes ACO, and **(d)** the proposed ADACO. A clear visual discrepancy exists between the predictions of the preceding methods and the ground-truth data. **(e)** Quantitative comparison of rose diagrams from the ADACO prediction (top) and the FMI log (bottom), demonstrating a high degree of consistency in the dominant NE-SW fracture orientation.

clarity. This approach uniquely employs dynamic probabilistic sampling of all anisotropy parameters (density, orientation, and credibility) and uses an HMM-guided path evaluation. By encoding uncertainty, ADACO adapts its search strategy, allowing it to thrive in geologically complex zones.

The final ADACO results (Fig. 13(c)) represent a breakthrough in fracture imaging. The algorithm exhibits a much higher resolution, showing a strong and continuous response to smaller-scale fractures in the 50–200 m range that were previously unresolved. Proximal to major fault traces, ADACO identifies highly dense fracture networks with clear, discernible intersecting strikes, which aligns strongly with the characteristics of fault damage zones. Crucially, the final network reveals clear geometric linkages between different structural scales, mapping how multiple smaller fractures converge towards or connect with major faults. This reflects the hierarchical nature of natural geologic structures and provides a complete, interconnected, and geologically realistic fracture system that aligns well with established geological principles.

3.5. Final validation against ground truth data

The ultimate test of the proposed algorithm is its corroboration with ground truth data from wellbores. The results from all three methods in our algorithmic progression—traditional ACO, ABACO, and ADACO—were rigorously validated against both direct drilling data and high-resolution formation micro imager (FMI) logs.

3.5.1. Drilling data verification: a comparative analysis

The most definitive validation of a fracture prediction is a direct comparison with fault locations physically encountered during drilling. We compared the predictions from all three algorithms with faults identified in eight horizontal wells drilled from platforms Y1H1 and Y1H3. The results, illustrated in Fig. 14, provide a stark, side-by-side comparison that unequivocally demonstrates the superiority of the ADACO method. To facilitate a clear and rigorous quantitative assessment, a drilled fault is considered successfully predicted only if two conditions are met: (1) a continuous algorithmic fracture trace passes within a 10-m radius of its location, and (2) this trace has a fracture probability greater than 0.5. This second criterion is crucial to ensure that a “hit” represents a confident prediction, not a coincidental overlap with low-probability algorithmic noise. Successfully predicted faults are highlighted with yellow diamonds in Fig. 14, while missed faults remain as red diamonds.

Fig. 14(a)–(c) show the results for platform Y1H1, while Fig. 14(d)–(f) show the results for Y1H3. The performance progression is striking:

- Traditional ACO (Fig. 14(a), (d)): This method serves as a baseline and is only capable of indicating some large-scale faults located outside the immediate well-pad area. Consequently, within the area of interest defined by the horizontal wells, it only successfully identifies 3 out of the 13 drilled faults, resulting in a low fault encounter rate of 23%. Its output shows no meaningful correlation with the majority of the drilled faults, establishing its inadequacy for detailed fracture characterization along the well path.
- ABACO (Fig. 14(b), (e)): By incorporating averaged anisotropy, ABACO's performance improves, correctly identifying 6 of the 13 faults for an encounter rate of 46%. However, it still fails to predict the majority of the ground-truth locations.
- ADACO (Fig. 14(c), (f)): ADACO exhibits excellent correspondence, successfully predicting 11 of the 13 drilled faults for a remarkable 85% encounter rate. The predicted fracture network not only aligns precisely with the yellow-marked locations but also reveals the continuous pathways connecting them.

This direct quantitative analysis, visually substantiated by the color-coded points in Fig. 14, confirms ADACO's superior locational accuracy. More importantly, while drilled faults represent discrete data points, the continuous network mapped by ADACO provides the crucial seismic prediction necessary for understanding fracture distribution far from the wellbore—an insight unattainable from drilling data alone.

3.5.2. FMI interpretation and comparison

Following the validation of locational accuracy, a detailed qualitative and quantitative validation was performed using formation micro imager (FMI) logs, which provide high-resolution measurements of fractures intersecting the wellbore. We present integrated validation panels for wells Y9 and Y1, contrasting the performance of all three algorithms against the ground-truth FMI data within their specific geological contexts.

The area around well Y9 is located on the southwestern limb of a syncline, a structurally complex setting with multiple nearby north-south trending thrust faults, as shown in the seismic profile in Fig. 15(a). Fig. 15(b)–(d) offer a side-by-side comparison of the fracture patterns predicted by each algorithm in the immediate vicinity of the well. A visual inspection clearly shows that the networks from traditional ACO (Fig. 15(b)) and ABACO (Fig. 15(c)) bear little resemblance to the dominant NE-SW fracture orientation revealed by the FMI log. In stark contrast, the ADACO prediction (Fig. 15(d)) accurately captures this complexity, revealing a high-density, multi-oriented network. This visual assessment is confirmed by the statistical orientation distributions in Fig. 15(e), which show a high degree of consistency between the ADACO-derived rose diagram and the FMI interpretation. Both show a prominent NE-SW peak, confirming ADACO's ability to identify the primary fracture orientation in a complex stress field.

In contrast, well Y1 is situated in an area of gentler, more open strata (Fig. 16(a)). Here, the side-by-side comparison shows that while the traditional ACO (Fig. 16(b)) and ABACO (Fig. 16(c)) results are sparse and poorly aligned, the ADACO-predicted fracture model (Fig. 16(d)) reveals a clear primary N-S to NNE-SSW trend with a significant secondary SE-NW orientation. This prediction aligns remarkably well with the multimodal distribution observed in the quantitative FMI comparison (Fig. 16(e)), further validating the reliability of the method across different structural settings.

This superior accuracy, now visually and statistically demonstrated in the integrated panels for both wells, underscores a clear hierarchy of performance. The fracture distributions predicted by ADACO show a strong and consistent correspondence with the FMI data. This stands in stark contrast to the preceding methods. While Ani-Bayes ACO (ABACO) captures some general trends, its results are often cluttered and inaccurate, failing to resolve the dominant fracture sets revealed by the logs. The traditional ACO method proves almost entirely ineffective at this scale, unable to identify any reliable fracture patterns that align with the ground-truth data. This result perfectly complements the drilling data validation, confirming that only ADACO excels in both locational accuracy and its ability to predict sub-seismic fractures with statistical distributions consistent with FMI data.

4. Discussion

The anisotropy-dynamic ant colony optimization (ADACO) algorithm constitutes a significant leap forward in seismic fracture detection, instituting a systematic revolution in data utilization, model construction, and optimization strategy. This evolution,

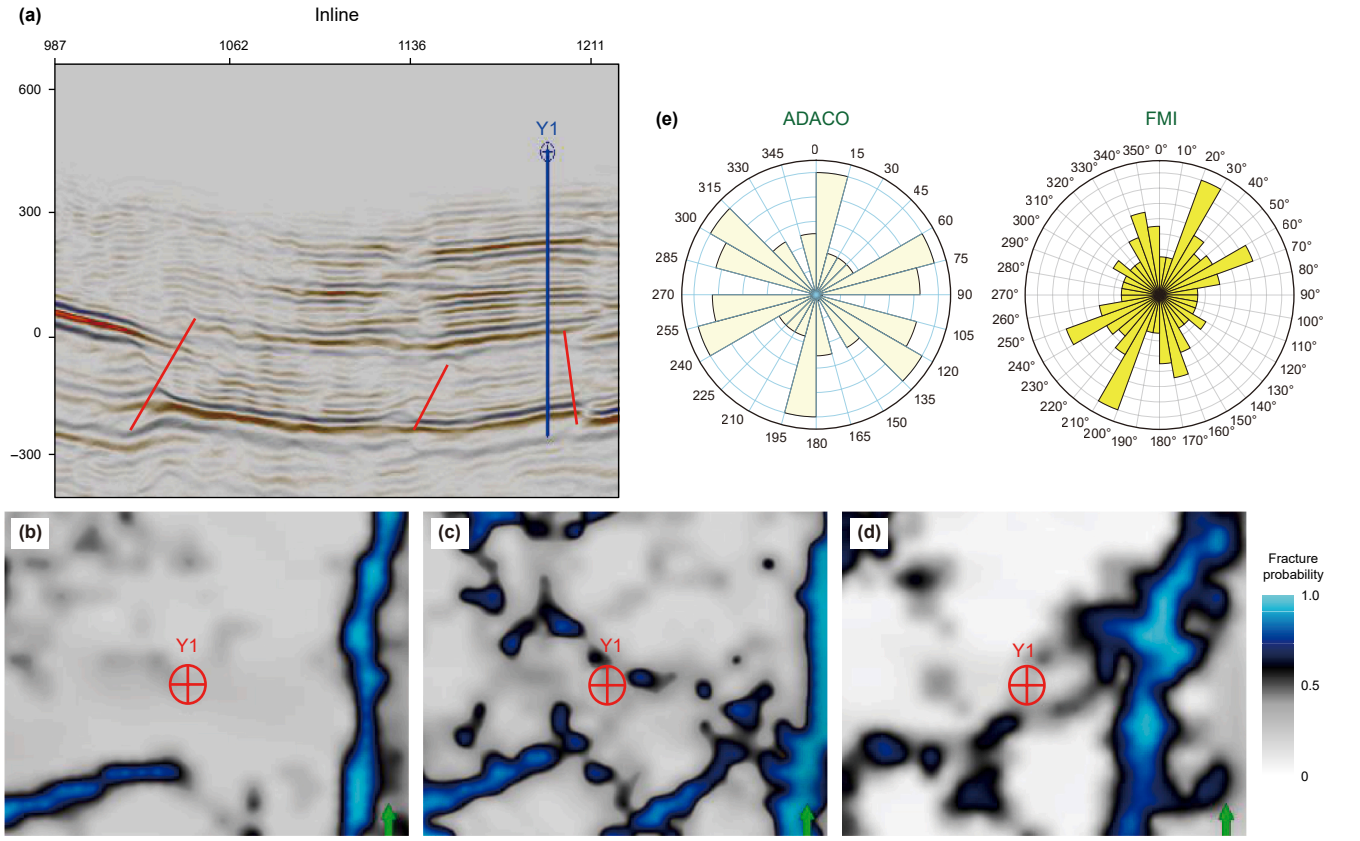

Fig. 16. Integrated validation panel at well Y1, situated in a region of gentler strata. **(a)** Seismic profile showing the well trajectory in a less deformed structural setting. **(b)**–**(d)** Side-by-side comparison of the fracture patterns predicted by **(b)** traditional ACO, **(c)** Ani-Bayes ACO, and **(d)** the proposed ADACO. The ADACO result reveals a much clearer and more detailed network. **(e)** Quantitative comparison of rose diagrams from the ADACO prediction (top) and the FMI log (bottom), revealing an excellent match for both the primary (N-S/NNE-SSW) and secondary (SE-NW) fracture orientations.

detailed in Table 3, moves beyond simple pattern recognition to intelligent optimization under robust geophysical constraints.

The superiority of ADACO stems from its leap from deterministic constraints to probabilistic modeling, which is actualized through a tightly coupled system of innovations. Unlike previous methods that treated geophysical attributes as infallible ground truth, ADACO's probabilistic framework handles them as information laden with uncertainty. This foundation is crucial, as it provides the HMM-based global evaluator with a realistic and uncertainty-aware search space to navigate. As highlighted in Table 3, this integrated design directly expands the algorithm's capability from detecting single-scale fractures to resolving multi-scale fracture networks with sub-seismic (sub-$\lambda/4$) resolution. Consequently, its ideal application shifts from simple corridors or coherent clusters to the highly complex multi-phase tectonic zones. The Zhaotong area exemplifies this: the algorithm correctly interpreted the ambiguity of low-credibility data not as noise, but as evidence of geological complexity, allowing it to resolve intersecting fracture patterns consistent with ground truth. This validates ADACO not merely as a tool for fracture delineation, but as a sophisticated and operationally viable methodology for resolving structural complexities in other challenging geological settings.

The implications of this integrated methodology for petroleum geosciences are profound. Beyond improved fracture mapping, ADACO's true significance lies in its holistic and robust framework for handling geophysical uncertainty. By synergizing probabilistic attribute modeling with globally-aware optimization, it provides a direct pathway for propagating data uncertainty into geological models—a critical step for quantitative risk assessment in reservoir development. This powerful, agent-based methodology, constrained by geological principles via the HMM, is potentially transferable to other challenging interpretation problems, such as delineating complex channel systems or salt bodies. As the industry moves towards greater geo-engineering integration, such integrated approaches that generate realistic, uncertainty-aware models are indispensable for optimizing field development strategies and maximizing economic returns.

5. Conclusion

This study presents ADACO, a novel anisotropy-dynamic ant colony optimization algorithm for seismic fracture detection. ADACO fundamentally advances prior ACO methods by replacing deterministic anisotropy constraints with probabilistic, credibility-weighted distributions (von Mises for orientation, log-normal for density) that dynamically evolve during optimization. Integrated with an HMM-based global path evaluator and iterative distribution focusing, this framework achieves three transformative capabilities: (1) uncertainty-quantified fracture intensity prediction, (2) simultaneous tracking of competing fracture sets through directional sampling, and (3) autonomous adaptation to multi-scale fracture clustering patterns. Application in the structurally complex Zhaotong shale gas reservoir demonstrated ADACO's superior resolution of sub-seismic fracture corridors, with drilling data validation confirming an 85% consistency rate—nearly doubling the performance of Ani-Bayes ACO (46%). FMI log comparisons further validated its accuracy in predicting

statistical fracture orientation distributions across varying structural settings.

ADACO bridges a critical gap between seismic-scale interpretation and sub-seismic fracture characterization. By probabilistically encoding pre-stack azimuthal anisotropy—including its inherent uncertainty—and enforcing global geological consistency, it delivers a robust, physically realistic fracture network model. This tool is particularly valuable for optimizing well placement and hydraulic fracturing design in complex reservoirs, where accurate sub-seismic fracture prediction directly impacts recovery efficiency. Future developments will focus on incorporating lithological controls and extending the HMM to hierarchically model fracture connectivity across scales.

CRediT authorship contribution statement

Shi-Chang Li: Writing – original draft. **Yang Zhao:** Writing – review & editing, Supervision. **Cheng-Gang Xian:** Writing – review & editing. **Qi-Ya Qiao:** Writing – review & editing. **Fu-Yu Zhu:** Supervision. **Xing Liang:** Supervision. **Jie-Hui Zhang:** Supervision. **Lan-Lan Yan:** Writing – review & editing.

Declaration of competing interest

No potential conflict of interest was reported by the authors.

Acknowledgement

The authors thank PetroChina Zhejiang Oilfield Company for permission to use the data and for operational insights. This research was jointly funded by the National Key R&D Program of China (Grant No. 2021YFA0716800), and the National Science and Technology Major Project for Oil and Gas Exploration and Development (Grant No. 2025ZD1401405), the National Natural Science Foundation of China (NSFC, Grant No. 42374064).

References

Acuña-Uribe, M., Pico-Forero, M.C., Goyes-Peñafiel, P., Mateus, D., 2021. Enhanced ant tracking: Using a multispectral seismic attribute workflow to improve 3D fault detection. Lead. Edge 40 (7), 502–512. https://doi.org/10.1190/tle40070502.1.

Al-Dossary, S., Marfurt, K.J., 2006. 3D volumetric multispectral estimates of reflector curvature and rotation. Geophysics 71 (5), P41–P51. https://doi.org/10.1190/1.2242449.

An, Y., Guo, J., Ye, Q., Childs, C., Walsh, J., Dong, R., 2021. Deep convolutional neural network for automatic fault recognition from 3D seismic datasets. Comput. Geosci. 153, 104776. https://doi.org/10.1016/j.cageo.2021.104776.

Ashraf, U., Zhang, H., Anees, A., Nasir Mangi, H., Ali, M., Ullah, Z., Zhang, X., 2020. Application of unconventional seismic attributes and unsupervised machine learning for the identification of fault and fracture network. Appl. Sci. 10 (11), 3864. https://doi.org/10.3390/app10113864.

Ashtari, A., 2025. Automating fault detection in seismic data: integrating image processing with deep learning. Appl. Comp. Geosci. 28, 100286. https://doi.org/10.1016/j.acags.2025.100286.

Asrillah, A., Abdullah, A., Bauer, K., Norden, B., Krawczyk, C.M., 2024. Fracture characterisation using 3-D seismic reflection data for advanced deep geothermal exploration in the NE German Basin. Geothermics 116, 102833. https://doi.org/10.1016/j.geothermics.2023.102833.

Bakulin, A., Grechka, V., Tsvankin, I., 2000. Estimation of fracture parameters from reflection seismic data—Part I: HTI model due to a single fracture set. Geophysics 65 (6), 1788–1802. https://doi.org/10.1190/1.1444863.

Cao, D., Han, J., Zeng, L., Huang, C., Bons, P.D., Liu, G.-P., Yao, Y.-T., Mao, Z., Lyu, W.-Y., Naaman, I., Zeng, L.-P., 2025. Natural fractures controlled by strike-slip faults in ultradeep carbonate reservoirs: A case study of the Middle and Lower Ordovician in the Tarim Basin, China. Pet. Sci. 22 (7), 2760–2776. https://doi.org/10.1016/j.petsci.2025.05.012.

Cao, H., Zhao, Y., Xian, C., Tang, H., Yan, L., Shuai, D., Zhang, L., Shen, Y., Li, S., 2024. Horizontal transverse isotropy anisotropic parameter inversion via azimuthal seismic velocity anisotropy and its application to anisotropic 3D in-situ stress estimation. Geophysics 89 (3), C105–C115. https://doi.org/10.1190/geo2023-0377.1.

Chen, G., Liu, W., Hurter, S., Zhao, P., Zhang, M., Liu, S., 2025. From edge detection to deep learning: image processing methods for seismic horizon tracking. Comput. Phys. Commun. 315, 109717. https://doi.org/10.1016/j.cpc.2025.109717.

Cheng, Z., Bian, L., Chen, H., Wang, X., Ye, D., He, L., 2022. Multiscale fracture prediction technique via deep learning, seismic gradient disorder, and aberrance: Applied to tight sandstone reservoirs in the Hutubi Block, southern Junggar Basin. Interpretation 10 (4), T647–T663. https://doi.org/10.1190/INT-2021-0249.1.

Choi, S., Lee, M.J., Jung, Y., Lee, J., Kim, J., Cho, Y., 2024. Enhancement of the consistency and connectivity of the ant-tracking algorithm via 3D U-net with dual-threshold iteration. Lithosphere 2024 (2), 118. https://doi.org/10.2113/2024/lithosphere_2024_118.

Dong, S., Zeng, L., Du, X., Bao, M., Lyu, W., Ji, C., Hao, J., 2022. An intelligent prediction method of fractures in tight carbonate reservoirs. Petrol. Explor. Dev. 49 (6), 1364–1376. https://doi.org/10.1016/S1876-3804(23)60355-6.

Durrani, M.Z.A., Rahman, S.A., Talib, M., Subhani, G., Sarosh, B., 2023. Azimuthal prestack seismic anisotropic inversion on a deep and tight carbonate reservoir from the North Potwar Basin of Pakistan. SPE Reservoir Eval. Eng. 26 (4), 1553–1565. https://doi.org/10.2118/215851-PA.

Guo, Z., Zhang, X., Liu, C., 2022. An improved scheme of azimuthally anisotropic seismic inversion for fracture prediction in volcanic gas reservoirs. IEEE Trans. Geosci. Rem. Sens. 60, 1–12. https://doi.org/10.1109/TGRS.2022.3186426.

Li, L., Zhang, G., Pan, X., Liu, J., 2021. Estimating effective stress parameter and fracture parameters in shale-gas fractured reservoirs using azimuthal fourier coefficients. Surv. Geophys. 42 (6), 1377–1400. https://doi.org/10.1007/s10712-021-09671-3.

Li, S., Zhao, Y., Xian, C., Liang, X., Zhang, J., Qiao, Q., Yan, L., Shen, Y., Cao, H., 2023. Small-scale fracture detection via anisotropic bayesian ant-tracking colony optimization driven by azimuthal seismic data. IEEE Trans. Geosci. Rem. Sens. 61, 1–12. https://doi.org/10.1109/TGRS.2023.3317313.

Liu, E., Zhang, F., Huo, S., Ding, P., Li, X., 2024. Viability of fracture characterization using seismic attributes through seismic physical modeling. J. Geophys. Eng. 21 (6), 1651–1666. https://doi.org/10.1093/jge/gxae094.

Liu, G., Jin, Z., Zeng, L., Chen, X., Ostadhassan, M., Mao, Z., Lu, J.-K., Cao, S., 2025. Natural fractures and their effectiveness in deep tight sandstone reservoirs of foreland thrust belts in the southern Junggar Basin, China. Pet. Sci. 22 (8), 3086–3100. https://doi.org/10.1016/j.petsci.2025.04.001.

Mavrovouniotis, M., Yang, S., Van, M., Li, C., Polycarpou, M., 2020. Ant colony optimization algorithms for dynamic optimization: A case study of the dynamic travelling salesperson problem [Research Frontier]. IEEE Comput. Intell. Mag. 15 (1), 52–63. https://doi.org/10.1109/MCI.2019.2954644.

Prakash, A., Al-Abdullah, M., Ali Faleh Naser, A.G., Mutlaq Mohammed, A.-O.T., Chakrabarti, B., Mulyono, R., Chilumuri, V., Thuwaini, A.-M., Al-Adwani, T.F., Mohamad Amar, A.N., Ahmad Homoud, A.-O., 2023. Exploring naturally fractured reservoirs: a case study. In: Third International Meeting for Applied Geoscience & Energy Expanded Abstracts, pp. 801–805. https://doi.org/10.1190/image2023-3910482.1.

Skackauskas, J., Kalganova, T., Dear, I., Janakiram, M., 2022. Dynamic impact for ant colony optimization algorithm. Swarm Evol. Comput. 69, 100993. https://doi.org/10.1016/j.swevo.2021.100993.

Tsvankin, I., Gaiser, J., Grechka, V., Van Der Baan, M., Thomsen, L., 2010. Seismic anisotropy in exploration and reservoir characterization: an overview. Geophysics 75 (5), 75A15–75A29. https://doi.org/10.1190/1.3481775.

Xie, W., He, G., Li, L., Jin, D., Chen, D., Zhang, H., Zhao, Y., 2020. Azimuthal anisotropy analysis of wide-azimuth P-wave seismic data for fracture orientation and density characterization in a tight gas reservoir. Interpretation 8 (1), SA73–SA83. https://doi.org/10.1190/INT-2019-0081.1.

Zhang, C., Hu, Z., Kong, X., Gao, B., Liu, J., Huang, Y., Chen, H., 2025. A comprehensive fracture characterization method for shale reservoirs. Pet. Sci. 22 (7), 2660–2676. https://doi.org/10.1016/j.petsci.2025.03.022.

Zhang, D., 2023. Comprehensive prediction of fractured carbonate reservoirs through logging-seismic integration. In: Lin, J. (Ed.), Proceedings of the International Field Exploration and Development Conference 2022, pp. 1554–1566. https://doi.org/10.1007/978-981-99-1964-2_134.

Zhang, G., Huang, X., Wu, L., Huang, X., Xu, Y., Wu, H., Tang, S., 2024a. Seismic-based workflow for multi-scale and multi-stage fracture characterization in the Longmaxi Formation, Weiyuan Gas Field, Sichuan Basin. Acta Geophys. 73 (3), 2391–2406. https://doi.org/10.1007/s11600-024-01503-3.

Zhang, L., Li, A., 2024. Study and application of wide-azimuth seismic anisotropy analysis and correction in shale reservoir in Gulong Sag, Songliao Basin, China. Geosci. J. 28 (6), 879–889. https://doi.org/10.1007/s12303-024-0040-2.

Zhang, X., Guo, Z., Liu, C., 2024b. Characterization of horizontal fractures in shale gas reservoirs using a rock-physics-based method integrated with SA-PSO algorithm and CNN. IEEE Trans. Geosci. Rem. Sens. 62, 1–14. https://doi.org/10.1109/TGRS.2024.3472057.

Zhang, Z., Zhang, T., Liu, H., Li, X., Xu, D., 2024c. Control and prediction of bedding-parallel fractures in fine-grained sedimentary rocks: A case from the Permian Lucaogou Formation in Jimusar Sag, Junggar Basin, Western China. Pet. Sci. 21 (6), 3815–3838. https://doi.org/10.1016/j.petsci.2024.09.003.

Zhou, X., Ma, H., Gu, J., Chen, H., Deng, W., 2022. Parameter adaptation-based ant colony optimization with dynamic hybrid mechanism. Eng. Appl. Artif. Intell. 114, 105139. https://doi.org/10.1016/j.engappai.2022.105139.